

## THERMAL INFRARED TECHNIQUE FOR LANDMINE DETECTION: MATHEMATICAL FORMULATION AND METHODS

NGUYEN TRUNG THÀNH, DINH NHO HÀO, AND HICHEM SAHLI

*Dedicated to Professor Tran Duc Van on the occasion of his sixtieth birthday*

ABSTRACT. This paper introduces a mathematical formulation of the problem of detection and characterization of shallowly buried landmines (more generally, buried objects) using passive thermal infrared technique. The problem consists of two steps. In the first step, referred to as *thermal modeling* which aims at predicting the soil temperature provided by the thermal properties of the soil and the buried objects, a parabolic partial differential equation based model is formulated. The proposed model is validated using experimental data. For solving the model, a splitting finite difference scheme is used. In the second step, referred to as *inverse problem setting for landmine detection*, the forward thermal model and acquired infrared images are used to detect the presence of buried objects and characterize them based on the estimation of their thermal and geometrical properties. Mathematically, this inverse problem is stated as the estimation of a piecewise constant coefficient of the heat transfer equation. To reduce the ill-posedness of this problem, which is due to the lack of spatial information in the measured data, we make use of a parametrization of the coefficient which needs only a small number of unknowns. The problem is then solved by gradient-based optimization methods. Numerical results both validate the proposed thermal model and illustrate the performance of the suggested algorithm for the inverse problem.

### 1. INTRODUCTION

Thermal infrared (IR) technique has been applied to the detection of shallowly buried landmines for more than a decade and has been found to be promising for non-metallic mines. Its aim is to detect and distinguish landmines from other buried objects (false alarms) using diurnal IR measurements of the air-soil interface. The detection principle is based on the perturbation of the ground temperature due to the presence of buried objects. Indeed, the presence of buried

---

Received February 14, 2011.

2000 *Mathematics Subject Classification.* 35K05, 35R05, 35R30, 65M06, 65M12.

*Key words and phrases.* Thermal infrared technique, landmine detection, heat equation, splitting methods, modeling, discontinuous coefficient identification.

The work was partly done when N.T. Thành and D.N. Hào were with Department of Electronics and Informatics, Vrije Universiteit Brussel.

The work of D.N. Hào was supported in part by NAFOSTED Grant 101.01.22.09.

objects, which have different properties compared to those of the soil, affects the diurnal heat conduction inside the soil. Consequently, the soil temperature on the ground above the objects is often different from that of the background. This temperature can be measured by an IR imaging system placed above the soil area. Figure 1 describes several heat transfer processes inside the soil and at the soil-air interface.

From measured thermal images, it is possible to detect the presence of shallowly buried anomalies using image processing techniques such as segmentation [6]. However, to classify them, one has to estimate their material properties (thermal diffusivity), size and shape. Such a problem is often solved in two steps. In the first step, referred to as *thermal modeling* which aims at predicting the soil temperature provided by the thermal properties of the soil and the buried objects, a parabolic partial differential equation based model is formulated. In the second step, referred to as *inverse problem setting for landmine detection*, the forward thermal model and acquired IR images are used to detect the presence of buried objects and characterize them based on the estimation of their thermal and geometrical properties.

The forward thermal model helps understanding the effect of buried objects on the soil-surface thermal signatures, while the inverse problem helps classifying the detected objects. So far, most of the works in IR technique for landmine detection have focused on defining and validating thermal models for buried landmines (see, e.g. [17, 24, 19]). However, there are just a few works considering the inverse problem [19, 31, 35, 33]. Mathematically, the inverse problem is stated as the estimation of a piecewise constant coefficient of the heat transfer equation from measurements on a surface of the boundary of the domain under investigation. Such problems have been discussed in some aspects in [2, 3, 4, 7, 8]. There are two main difficulties in dealing with this problem: (i) it is extremely difficult to have a thermal model which is valid under different soil and weather conditions; (ii) the lack of spatial information in observed data since it is only taken at the air-soil interface while the coefficient needed to be estimated is a three-dimensional function. This is different from most of the publications on this topic in the literature in which the measured data is available on the whole boundary or even in the whole domain (see, e.g., [11, 12, 14]).

Note that IR cameras do not measure the temperature of the soil surface itself but the thermal radiation emitted from the soil surface. In order to use the measured IR images in thermal modeling, a pre-processing chain, consisting of: 1) radiometric calibration; 2) temporal co-registration; 3) apparent temperature conversion; and 4) inverse perspective (ground) projection, must be applied. The output of this pre-processing chain is an image sequence of the soil-surface apparent temperature. A detailed description of the pre-processing steps is given in [6]. In this work, we consider the measured IR images as the soil-surface temperature measured during the period of analysis.

In [34] we proposed and validated a thermal model with the estimation of soil thermal properties from *in situ* measurements. This approach enables us to apply the thermal model in a wide range of soil and weather conditions. In

[35, 33] the inverse problem was investigated. In these papers, keeping in mind our application to buried landmine detection, we assumed that buried objects were upright cylinders, but their horizontal cross-sections were not necessarily circular. Under these assumptions, a buried object was specified by (i) its depth of burial, (ii) its height, (iii) its horizontal cross-section, and (iv) its thermal diffusivity. Then a two step method was proposed to solve the inverse problem. In the first step, we considered a given cross-section which was obtained by image segmentation techniques [35], and we estimated three parameters, namely, the depth of burial, the height, and the thermal diffusivity. This approach helps reducing the ill-posedness of the estimation problem as it reduces the number of unknown parameters. However, its result depends on the accuracy of the cross-section being given by the anomaly detection procedures. In the second step, we used the result of the previous step as an initial guess for estimating the full parameter vector, namely, the depth of burial, the height and the thermal diffusivity on a horizontal plane of the soil domain across the object. The cross-section was improved via the estimated thermal diffusivity on this plane. This step helps improving the result of the first step.

This paper gives a review of our previous works [31, 32, 33, 34, 35] with new contributions. It is different from the above ones in two points. First, we propose a slightly different thermal model. Second, in solving the inverse problem, we make use of another parametrization method to represent the shape of the object. More precisely, we also assume that the object is an upright cylinder with a star-shaped cross-section. In this case, the cross-section can be parametrized by Fourier coefficients of its radial function. If the cross-section is regular, the number of Fourier coefficients to be estimated can be significantly reduced. For example, only one parameter is needed for a circular cross-section. Using this parametrization method we only need to estimate a small number of unknowns. This makes the inverse problem more stable.

To solve the inverse problem, we also use gradient-based iterative methods as in [35, 33]. An estimate of the object's cross-section using the image segmentation technique described in [35] is used as an initial guess for the iterative method.

The rest of the paper is organized as follows. In Section 2, we describe the mathematical formulation of the thermal modeling and discuss its well-posedness. In this section we also propose a finite difference splitting scheme for solving the thermal model and prove its convergence. Section 3 is devoted to the inverse problem which is stated as a minimization problem using the least-squares approach. The gradient of the objective function is given and the parametrization of the object's shape is described. In Section 4, we validate the proposed thermal model for experimental data and illustrate the performance of the algorithm for the inverse problem with both simulated and experimental data. Finally, some conclusions and perspectives are given in Section 5.

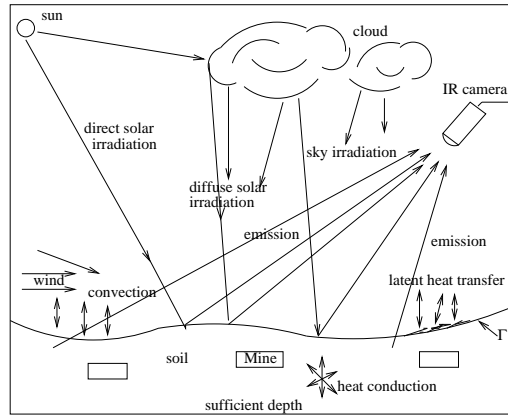


FIGURE 1. Heat transfer processes inside the soil and on the air-soil interface.

2. FORWARD THERMAL MODELING FOR LANDMINE DETECTION

The principle of the IR technique for landmine (more generally, buried object) detection is based on unusual diurnally temperature signatures on the ground surface due to the presence of buried objects. The change in the ground temperature depends not only on the ground properties and heating conditions but also on the physical properties, size and depth of burial of the buried objects. Understanding how these parameters affect the ground temperature is crucial to the detection and classification process. This is the objective of the forward modeling. In this section, we formulate a mathematical model approximating the ground temperature given a buried landmine (object) under natural heating conditions. The model is described as an initial boundary value problem for the heat equation.

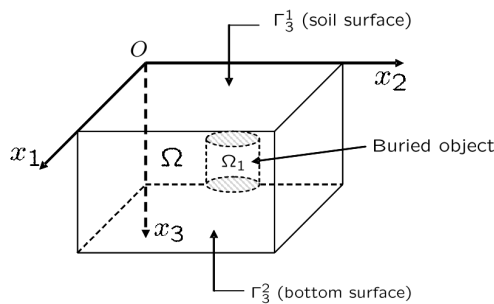


FIGURE 2. Orthonormal Cartesian coordinate system associated with the soil volume.

2.1. **Mathematical formulation of the thermal model.** For simplicity, we assume that the ground surface in a small area is flat (see Remark 2.2). Within

this area, let us consider a rectangular parallelepiped  $\Omega$ , which contains a buried landmine as shown in Figure 2. We associate the soil volume with an orthonormal Cartesian coordinate system in which the coordinate of a point is denoted by  $x := (x_1, x_2, x_3)'$ . Without loss of generality, we assume that  $\Omega := \{x : 0 < x_i < l_i, i = 1, 2, 3\}$ . We denote by  $\Gamma$  the boundary of  $\Omega$ . We also denote by  $\Gamma^1$  the ground surface – the only part of  $\Gamma$  which is accessible for IR measurements – and  $\Gamma^2 := \Gamma \setminus \Gamma^1$ . The duration of analysis is denoted by  $(0, t_e)$  and  $S_{t_e}^i := \Gamma^i \times (0, t_e), i = 1, 2$ . In this work, we assume that the soil and the mine are isotropic and thermally homogeneous. Moreover, the soil moisture content variation is assumed to be negligible during the period of analysis. Then the temperature distribution  $T(x, t), (x, t) \in \mathbb{Q}_{t_e} := \Omega \times (0, t_e)$ , can be approximated by the solution to the following parabolic partial differential equation [5, 29]

$$(2.1) \quad \frac{\partial T}{\partial t} = \sum_{i=1}^3 \frac{\partial}{\partial x_i} \left( \alpha(x) \frac{\partial T}{\partial x_i} \right), \quad \forall (x, t) \in \mathbb{Q}_{t_e},$$

where  $\alpha(x)$  ( $\text{m}^2/\text{s}$ ) is the thermal diffusivity (of the soil and the buried mine) in the domain.

2.1.1. *Initial and boundary conditions.* In order to solve (2.1), one has to know the initial temperature distribution as well as necessary boundary conditions, e.g. the prescribed soil temperature or incoming heat flux on the boundary  $\Gamma$  of the domain. These conditions are described in the following.

1. The initial condition expresses the temperature distribution in  $\Omega$  at the beginning of analysis

$$(2.2) \quad T(x, 0) = g(x), \quad x \in \Omega.$$

We note that, in practice, the initial soil temperature distribution  $g(x)$  is generally not known in an arbitrary minefield. In [31, 34], we approximated it by interpolations from the measured soil temperature at a reference location. This temperature is measured at different depths. In doing so, we made use of the assumption that the temperature of the mine is almost the same as that of the surrounding soil. However, this assumption is reasonable only at some certain time instants such as around sunrise or sunset [19, 31]. Therefore, we should start the analysis in these time periods.

2. On the ground surface, there are different heat transfer processes resulting in an incoming heat flux given by

$$(2.3) \quad \kappa_s \frac{\partial T}{\partial n}(x, t) = q_{net}(x, t), \quad (x, t) \in S_{t_e}^1,$$

where  $n$  is the outward unit normal vector to  $\Gamma$  and  $\kappa_s$  ( $\text{W}/\text{m}/\text{K}$ ) is the soil thermal conductivity. In this work, we assume that the evaporation/condensation is negligible during the period of analysis, so the surface heat flux (2.3) can be approximated as follows [36, 16]

$$(2.4) \quad q_{net}(x, t) = q_{sun}(t) + q_{sky}(t) + q_{conv}(x, t) - q_{emis}(x, t),$$

where

- $q_{sun} := \epsilon_{sun} E_{sun}$  (W/m<sup>2</sup>) is the solar irradiance absorbed by the soil with  $\epsilon_{sun}$  being the *solar absorption coefficient* of the soil and  $E_{sun}$  (W/m<sup>2</sup>) the *solar irradiance* on the earth's surface.
- $q_{sky} := \epsilon_{sky} E_{sky}$  (W/m<sup>2</sup>) is the sky irradiance absorbed by the soil with  $\epsilon_{sky}$  being the *sky absorption coefficient* of the soil and  $E_{sky}$  (W/m<sup>2</sup>) the *sky irradiance* on the earth's surface.
- $q_{conv}$  (W/m<sup>2</sup>) is the heat transfer by convection between the soil and the air. It refers to the transport of heat between the soil surface and the atmosphere by motion of the air.
- $q_{emis}$  (W/m<sup>2</sup>) is the thermal emittance of the soil. It corresponds to the thermal radiation emitted by the soil surface.

In practice, the solar irradiance  $E_{sun}$  and the sky irradiance  $E_{sky}$  are either approximated using model formulas [36, 16] or measured via a weather station placed near the minefield [6]. Comparisons between the models and measured data were discussed in [34]. In this work, we use the latter method in order to avoid possible inaccuracies of the models in real situations.

From Stefan–Boltzmann's law [16], the thermal emittance is given by

$$(2.5) \quad q_{emis}(x, t) = \epsilon_{soil} \sigma T^4(x, t), \quad (x, t) \in S_{t_e}^1,$$

with  $\epsilon_{soil}$  being the soil thermal emissivity and  $\sigma = 5.67 \times 10^{-8}$  (W/m<sup>2</sup>/K<sup>4</sup>) being Stefan–Boltzmann's constant.

The convection term in (2.4) is usually approximated by Newton's law [5]

$$(2.6) \quad q_{conv}(x, t) = h_{conv} [T_{air}(t) - T(x, t)], \quad (x, t) \in S_{t_e}^1,$$

where  $h_{conv}$  (W/m<sup>2</sup>/K) is the convective heat transfer coefficient and  $T_{air}$  is the air temperature. In general, the convective heat transfer coefficient depends on wind speed. Consequently, it varies from time to time and is difficult to be accurately approximated. In this work, for simplicity, we assume that the model is only applicable in the absence of strong wind, so the coefficient  $h$  can be considered as a constant which can be estimated using in situ measurements, see [34, 31].

From (2.4)–(2.6) the heat flux at the air-soil interface is rewritten as

$$(2.7) \quad \begin{aligned} q_{net}(x, t) &= \epsilon_{sun} E_{sun}(t) + \epsilon_{sky} E_{sky}(t) \\ &\quad - \epsilon_{soil} \sigma T^4(x, t) + h_{conv} [T_{air}(t) - T(x, t)], \quad (x, t) \in S_{t_e}^1. \end{aligned}$$

3. On the part  $\Gamma^2$  of the boundary, we assume that the considered domain is large and deep enough so that the effect of the landmine on the bottom and vertical boundary surfaces can be neglected. In this case, under the assumption of homogeneous soil, the heat balance takes place on  $\Gamma^2$ . This condition is described by the equation

$$(2.8) \quad \frac{\partial T}{\partial n}(x, t) = 0 \quad \text{for } (x, t) \in S_{t_e}^2.$$

Equation (2.1) with conditions (2.2)–(2.8) is considered as the thermal model of the soil with the presence of shallowly buried landmines.

**Remark 2.1.** Concerning the boundary condition at the bottom of the soil volume, we can also assume that the soil temperature at a sufficiently deep depth is constant in the period of analysis which results in the Dirichlet boundary condition. This condition was used in our previous papers [34, 35, 33].

2.1.2. *Linearization.* We note that the thermal model (2.1)–(2.8) is nonlinear due to the nonlinearity of the boundary condition (2.7) on the air-soil interface. Therefore, solving this problem is really time-consuming. To overcome this difficulty, the nonlinear condition is usually linearized. In the literature, the linearization has been performed using the modeled sky irradiance [36, 24]. In this work, the linearization is performed by approximating the soil thermal emittance term (2.5) by the following form

$$(2.9) \quad q_{emis}(x, t) = \epsilon_{soil}\sigma T^4(x, t) \approx \epsilon_{soil}\sigma T_0^4 + 4\epsilon_{soil}\sigma T_0^3 [T(x, t) - T_0],$$

if  $\frac{T(x,t)-T_0}{T_0} \ll 1$ . The value  $T_0$  may be chosen as the mean value of the soil surface temperature measured by, e.g. a thermocouple. From (2.3), (2.7) and (2.9) we have

$$(2.10) \quad \alpha_s \frac{\partial T(x, t)}{\partial n} + pT(x, t) = q(t), \quad (x, t) \in S_{te}^1,$$

with  $\alpha_s$  (m<sup>2</sup>/s) being the thermal diffusivity of the homogeneous soil and

$$(2.11) \quad \begin{aligned} p &:= \frac{\alpha_s}{\kappa_s} (4\epsilon_{soil}\sigma T_0^3 + h_{conv}), \\ q(t) &:= \frac{\alpha_s}{\kappa_s} [\epsilon_{sun} E_{sun}(t) + \epsilon_{sky} E_{sky}(t) + 3\epsilon_{soil}\sigma T_0^4 + h_{conv} T_{air}(t)]. \end{aligned}$$

Here  $E_{sun}$ ,  $E_{sky}$ ,  $T_0$  and  $T_{air}$  are measured values. In (2.10), we have multiplied both sides by  $\alpha_s/\kappa_s$  for the convenience of mathematical analysis and numerical methods presented in the sequel.

In summary, we have the following linearized forward thermal model of shallowly buried objects

$$(2.12) \quad \begin{cases} \frac{\partial T}{\partial t}(x, t) - \sum_{i=1}^3 \frac{\partial}{\partial x_i} \left( \alpha(x) \frac{\partial T(x, t)}{\partial x_i} \right) = 0, & (x, t) \in \mathbb{Q}_{te}, \\ \alpha(x) \frac{\partial T}{\partial n}(x, t) + pT(x, t) = q(t), & (x, t) \in S_{te}^1, \\ \frac{\partial T}{\partial n}(x, t) = 0, & (x, t) \in S_{te}^2, \\ T(x, 0) = g(x), & x \in \Omega, \end{cases}$$

**Remark 2.2.** Above we assumed that the soil is isotropic and homogeneous and the soil surface is flat. Moreover, the moisture content variation and the evaporation/condensation are negligible during the period of analysis. These assumptions, of course, are not accurate under all soil and weather conditions. However, in our application, we assume that the thermal model can only be applied under reasonably good weather conditions such as dry climates with the absence of strong wind or rain. Under these conditions, the assumptions on the moisture content variation and the evaporation/condensation are acceptable. In addition, we only consider a small soil volume, say, 50 cm by 50 cm by 50 cm

around each mine. Within such a small area, the assumptions on the homogeneity of the soil and flat soil surface are acceptable. These assumptions have also been made in the literature (see, e.g. [17, 24, 20] and the references therein).

Under the assumption of homogeneous soil and mine, the thermal diffusivity  $\alpha(x)$  is piecewise constant, that is

$$\alpha(x) = \begin{cases} \alpha_o, & x \in \Omega_1, \\ \alpha_s, & x \in \Omega \setminus \Omega_1, \end{cases}$$

where  $\alpha_o$  is the thermal diffusivity of the mine and  $\Omega_1$  is the sub-domain of  $\Omega$  occupied by the mine.

**Remark 2.3.** In practical applications, it should be remarked that the soil thermal diffusivity  $\alpha_s$  and the parameters  $p$  and  $q$  in (2.11) are generally not available. Moreover, it is not easy to measure these parameters in an arbitrary minefield. In our approach, these parameters are estimated using in situ measurements. More precisely, the soil thermal diffusivity can be estimated using measured soil temperature profiles at different depths at a reference location. The estimation of  $\alpha_s$  is then treated as a 1D coefficient reconstruction problem. The surface coefficients  $p$  and  $q(t)$  are estimated from the ground temperature measured by the IR camera using a 1D model with homogeneous soil. For more details, we refer the reader to [31, 34].

**2.2. Well-posedness of the forward thermal model.** Since the coefficient  $\alpha(x)$  is discontinuous, problem (2.12) does not have solutions in the classical sense. We therefore introduce the notion of generalized solutions defined in the Sobolev space  $H^{1,1}(\mathbb{Q}_{t_e})$ . For definitions and properties of Sobolev spaces, we refer the reader to [1, 18]. The generalized solutions of the thermal model (2.12) are defined as follows.

**Definition 2.4.** A function  $T(x, t)$  is called a generalized solution of (2.12) in the Sobolev space  $H^{1,1}(\mathbb{Q}_{t_e})$  if it belongs to this space and satisfies the following problem

$$(2.13) \quad \begin{cases} \int_{\mathbb{Q}_{t_e}} T_t \eta dx dt + \int_{\mathbb{Q}_{t_e}} \alpha T_x \eta_x dx dt + \int_{S_{t_e}^1} p T \eta dx_3' dt = \int_{S_{t_e}^1} q \eta dx_3' dt, \quad \forall \eta \in H^{1,0}(\mathbb{Q}_{t_e}), \\ T(x, 0) = g(x), \quad x \in \Omega, \end{cases}$$

where  $dx_3' := dx_1 dx_2$  and  $T_x \eta_x := \sum_{i=1}^3 T_{x_i} \eta_{x_i}$ .

For a general interest, in this section we consider problem (2.12) with the right hand side of the governing equation being set to be  $f(x, t)$ , i.e. the following

problem

$$(2.14) \quad \begin{cases} \int_{\mathbb{Q}_{t_e}} u_t \eta dx dt + \int_{\mathbb{Q}_{t_e}} \alpha u_x \eta_x dx dt + \int_{S_{t_e}^1} p u \eta dx_3' dt \\ = \int_{\mathbb{Q}_{t_e}} f \eta dx dt + \int_{S_{t_e}^1} q \eta dx_3' dt, \forall \eta \in H^{1,0}(\mathbb{Q}_{t_e}), \\ u(x, 0) = g(x), \quad x \in \Omega. \end{cases}$$

The well-posedness of the problem (2.14) is stated in the following theorem. Its proof is demonstrated in [31].

**Theorem 2.5.** *For problem (2.14) suppose that*

- (1)  $\alpha \in L_\infty(\Omega) : 0 < \nu \leq \alpha(x) \leq \mu$ , for a.e.  $x \in \Omega$ ,
- (2)  $p > 0$ ,  $f \in L_2(\mathbb{Q}_{t_e})$ ,  $q \in H^1(0, t_e)$ ,  $g(x) \in H^1(\Omega)$ .

*Then it has a unique solution  $u$  in  $H^{1,1}(\mathbb{Q}_{t_e})$ . Moreover, this solution satisfies the energy balance inequality*

$$(2.15) \quad \|u\|_{H^{1,1}(\mathbb{Q}_{t_e})} \leq C (\|q\|_{H^1(0,t_e)} + \|g\|_{H^1(\Omega)} + \|f\|_{L_2(\Omega)}),$$

*where  $C$  is a positive constant independent of  $u$ .*

**2.3. A splitting numerical method for solving the forward thermal model.** In our approach, we apply the finite difference method proposed by Ladyzhenskaya [18] for solving the thermal model (2.12). The method introduces difference schemes based on the integral equation corresponding to the definition of the generalized solution instead of the original differential equation. The convergence of approximate solutions to the generalized one of the original problem is proved based on embedding theorems of interpolations of grid functions. The method consists of two steps. First, we approximate the original problem (2.12) by a system of ordinary differential equations of the time variable  $t$  by discretizing the problem in the space variable  $x$ . Then a splitting scheme is introduced for solving the system (see [21, 22, 27] and the references therein). To prove the convergence of the difference scheme to the solution of the original problem we need to recall some properties of interpolations of grid functions. For further discussions, we refer the reader to [18], Chapter 6.

**2.3.1. Interpolations of grid functions.** We divide the domain  $\Omega$  into small cells by the planes  $\{x_i = k_i h_i\}$  with  $k_i = 0, 1, \dots, N_i$ ,  $h_i = l_i/N_i$ . To simplify the notation, we set  $x(k) := (k_1 h_1, k_2 h_2, k_3 h_3)'$ ,  $k := (k_1, k_2, k_3)$ ,  $k+1 := (k_1+1, k_2+1, k_3+1)$ ;  $h := (h_1, h_2, h_3)'$  and  $\Delta h := h_1 h_2 h_3$ . We also denote by  $e_i$  the unit normal vector along the  $x_i$ -direction in  $\mathbb{R}^3$ , i.e.  $e_1 := (1, 0, 0)'$  and so on. In the following, we need to use the following subsets of  $\Omega$

$$\begin{aligned} \omega^+(k) &:= \{x \in \Omega : k_i h_i \leq x_i \leq (k_i + 1) h_i, \quad i = 1, 2, 3\}, \\ \omega(k) &:= \{x \in \Omega : (k_i - 0.5) h_i \leq x_i \leq (k_i + 0.5) h_i, \quad i = 1, 2, 3\}, \\ \omega_i^+(k) &:= \{x \in \Omega : k_i h_i \leq x_i \leq (k_i + 1) h_i, (k_j - 0.5) h_j \leq x_j \leq (k_j + 0.5) h_j, \quad \forall j \neq i\}. \end{aligned}$$

The set of the indices of grid points belonging to  $\bar{\Omega}$  is denoted by  $\bar{\Omega}_h$ . That is,

$$\bar{\Omega}_h := \{k : 0 \leq k_i \leq N_i, i = 1, 2, 3\}.$$

The following subsets of  $\bar{\Omega}_h$  will also be used in the sequel

$$\bar{\Omega}_i^- := \{k : 0 \leq k_i \leq N_i - 1, 0 \leq k_j \leq N_j, \forall j \neq i\}.$$

Suppose that  $u^h(k, t)$  is a grid function defined in  $\mathbb{Q}_{ht_e} := \bar{\Omega}_h \times (0, t_e)$  having the generalized derivative with respect to  $t$ . Moreover, the following norm (2.16)

$$\|u^h\|_{H^{1,1}(\mathbb{Q}_{ht_e})}^2 := \Delta h \int_0^{t_e} \left\{ \sum_{k \in \bar{\Omega}_h} \left( [u^h(k, t)]^2 + [u_t^h(k, t)]^2 \right) + \sum_{i=1}^3 \sum_{k \in \bar{\Omega}_i^-} [u_{x_i}^h(k, t)]^2 \right\} dt$$

is assumed to be bounded by a constant which is independent of  $h$ , with

$$u_{x_i}^h(k) := \frac{u^h(k + e_i) - u^h(k)}{h_i}$$

being the forward difference quotient of the grid function  $u^h$ . We also define the backward difference quotient of  $u$  by

$$u_{\bar{x}_i}^h(k) := \frac{u^h(k) - u^h(k - e_i)}{h_i}.$$

For the grid function  $u^h(k, t)$  we define the following interpolations in  $\mathbb{Q}_{t_e}$

$$(2.17) \quad \tilde{u}^h(x, t) := u^h(k, t), \quad (x, t) \in \omega(k) \times (0, t_e),$$

(2.18)

$$\begin{aligned} \hat{u}^h(x, t) := & u^h(k, t) + \sum_{i=1}^3 u_{x_i}^h(k)(x_i - k_i h_i) + \sum_{1 \leq i < j \leq 3} u_{x_i x_j}^h(k)(x_i - k_i h_i)(x_j - k_j h_j) \\ & + u_{x_1 x_2 x_3}^h(k) \prod_{i=1}^3 (x_i - k_i h_i), \quad (x, t) \in \omega^+(k) \times (0, t_e). \end{aligned}$$

It is clear from (2.17) and (2.18) that the interpolation  $\tilde{u}^h$  is constant in each subdomain  $\omega(k)$  while  $\hat{u}^h$  is multi-linear in  $\omega^+(k)$ . Moreover,  $\hat{u}^h$  belongs to  $H^{1,1}(\mathbb{Q}_{t_e})$ . We have the following properties of the multi-linear interpolation.

**Lemma 2.6.** *Suppose that for the grid function  $u^h$  we have*

$$(2.19) \quad \|u^h\|_{H^{1,1}(\mathbb{Q}_{ht_e})} \leq C,$$

where  $C$  is a constant independent of  $h$ . Then the multi-linear interpolation (2.18) is bounded in the norm of  $H^{1,1}(\mathbb{Q}_{t_e})$ .

Asymptotic relationships between the two interpolations as  $h$  tends to zero are stated in the following lemmas.

**Lemma 2.7.** *Suppose that the hypothesis of Lemma 2.6 is fulfilled. Then if  $\{\hat{u}^h(x, t)\}_h$  converges strongly to a function  $u(x, t)$  in  $L_2(\mathbb{Q}_{t_e})$  as the grid size  $h$  tends to zero, the sequence  $\{\tilde{u}^h(x, t)\}_h$  also converges to  $u(x, t)$  in the same manner. Moreover, the assertion is still valid for the projections of the functions*

on the boundary of  $\Omega$ , i.e. if  $\{\hat{u}_{|\Gamma}^h\}_h$  converges to  $u_{|\Gamma}$ ,  $\{\tilde{u}_{|\Gamma}^h\}_h$  also converges to  $u_{|\Gamma}$ .

**Lemma 2.8.** *Suppose that the hypothesis of Lemma 2.6 is fulfilled and  $i \in \{1, 2, 3\}$ . Then if the sequence of derivatives  $\{\hat{u}_{x_i}^h(x, t)\}_h$  converges weakly to a function  $v(x, t)$  in  $L_2(\mathbb{Q}_{t_e})$  as  $h$  tends to zero, the sequence  $\{\tilde{u}_{x_i}^h(x, t)\}_h$  also converges to  $v(x, t)$  in the same manner, where*

$$\tilde{u}_{x_i}^h(x, t) := u_{x_i}^h(k), \quad \forall x \in \omega_i^+(k).$$

For the proofs of the above lemmas, we refer the reader to [18], Chapter 6, §6.3 and §6.4.

2.3.2. *Spatial discretization.* In addition to the notation in §2.3.1, we also need the following notation

$$\bar{\Gamma}_h^1 := \{k = (k_1, k_2, 0) : 0 \leq k_i \leq N_i, \quad \forall i = 1, 2\}.$$

Suppose that  $u^h(k, t)$  is a grid function defined on  $\mathbb{Q}_{t_e}$ . In this section, we drop the time variable  $t$  for simplifying the notation, i.e.  $u^h(k, t)$  is abbreviated by  $u^h(k)$ . The integrals in (2.14) with respect to  $x$  are approximated formally as follows

$$\begin{aligned} \int_{\Omega} \alpha u_{x_i} \eta_{x_i} dx dt &\approx \Delta h \sum_{k \in \bar{\Omega}_i^-} \alpha_i^+(k) u_{x_i}^h(k) \eta_{x_i}^h(k), \quad i = 1, 2, 3, \\ \int_{\Gamma^1} u \eta dx'_3 &\approx h_1 h_2 \sum_{k \in \bar{\Gamma}_h^1} u^h(k) \eta^h(k), \\ \int_{\Omega} f \eta dx &\approx \Delta h \sum_{k \in \bar{\Omega}_h} f^h(k) \eta^h(k), \end{aligned}$$

where  $u^h(k)$  and  $\eta^h(k)$  are respectively certain types of approximations of  $u$  and  $\eta$  at the point  $x = kh$ . In the following, we denote  $u^h = \{u^h(k), k \in \bar{\Omega}_h\}$ . The quantities  $f^h(k)$  and  $\alpha_i^+(k)$  are the mean values in the corresponding cells

$$\begin{aligned} f^h(k) &:= \frac{1}{|\omega(k)|} \int_{\omega(k)} f(x) dx, \quad k \in \bar{\Omega}_h, \\ \alpha_i^+(k) &:= \frac{1}{|\omega_i^+(k)|} \int_{\omega_i^+(k)} \alpha(x) dx, \quad k \in \bar{\Omega}_i^-. \end{aligned}$$

With the above approximations, we have the following discrete analogue of the first equation of (2.14)

$$(2.20) \quad \begin{aligned} & \Delta h \int_0^{t_e} \left[ \sum_{k \in \bar{\Omega}_h} u_t^h(k) \eta^h(k) + \sum_{i=1}^3 \sum_{k \in \bar{\Omega}_i^-} \alpha_i^+(k) u_{x_i}^h(k) \eta_{x_i}^h(k) + \frac{1}{h_3} \sum_{k \in \bar{\Gamma}_h^1} p u^h(k) \eta^h(k) \right] dt \\ &= \Delta h \int_0^{t_e} \sum_{k \in \bar{\Omega}_h} f^h(k) \eta(k) dt + h_1 h_2 \int_0^{t_e} \sum_{k \in \bar{\Gamma}_h^1} q \eta^h(k) dt, \end{aligned}$$

for all grid functions  $\eta(k, t)$  satisfying  $\eta(k, \cdot) \in L_2(0, t_e)$ ,  $\forall k \in \bar{\Omega}_h$ . For arbitrary but fixed values  $k_2, k_3$  satisfying  $0 \leq k_2 \leq N_2$  and  $0 \leq k_3 \leq N_3$ , we have

$$\begin{aligned} \sum_{k_1=1}^{N_1-1} \alpha_1^+(k) u_{x_1}^h(k) \eta_{x_1}^h(k) &= - \frac{\alpha_1^+(0, k_2, k_3) u_{x_1}^h(0, k_2, k_3)}{h_1} \eta^h(0, k_2, k_3) \\ &+ \sum_{k_1=1}^{N_1-1} \frac{\alpha_1^-(k) u_{x_1}^h(k) - \alpha_1^+(k) u_{x_1}^h(k)}{h_1} \eta^h(k) \\ &+ \frac{\alpha_1^-(N_1, k_2, k_3) u_{x_1}^h(N_1, k_2, k_3)}{h_1} \eta^h(N_1, k_2, k_3), \end{aligned}$$

with  $\alpha_1^-(k) = \alpha_1^+(k - e_1)$ . The same manner is applied to the two other terms in the  $x_2$ - and  $x_3$ -directions. From these equalities, (2.14) is approximated by the following system

$$(2.21) \quad \begin{cases} \int_0^{t_e} [u_t^h + (\mathcal{A}_1 + \mathcal{A}_2 + \mathcal{A}_3) u^h - F^h](k, t) \eta(k, t) dt = 0, \quad \forall \eta(k, \cdot) \in L_2(0, t_e), \quad k \in \bar{\Omega}_h, \\ u^h(k, 0) = g^h(k), \quad k \in \bar{\Omega}_h, \end{cases}$$

with  $g^h(k) := \frac{1}{|\omega(k)|} \int_{\omega(k)} g(x) dx$ , the average value of  $g(x)$  in the corresponding subdomain, and the operators specified by

$$(2.22) \quad (\mathcal{A}_i u^h)(k) := \begin{cases} \frac{\alpha_i^-(k) u_{x_i}^h(k)}{h_i} - \frac{\alpha_i^+(k) u_{x_i}^h(k)}{h_i}, & 1 \leq k_i \leq N_i - 1, \\ -\frac{\alpha_i^+(k)}{h_i} u_{x_i}^h(k), & k_i = 0, \\ \frac{\alpha_i^-(k)}{h_i} u_{x_i}^h(k), & k_i = N_i \end{cases}$$

for  $i = 1, 2$  and

$$(2.23) \quad (\mathcal{A}_3 u^h)(k) := \begin{cases} \frac{\alpha_3^-(k) u_{x_3}^h(k)}{h_3} - \frac{\alpha_3^+(k) u_{x_3}^h(k)}{h_3}, & 1 \leq k_3 \leq N_3 - 1, \\ -\frac{\alpha_3^+(k) u_{x_3}^h(k)}{h_3} + \frac{p u^h(k)}{h_3}, & k_3 = 0, \\ \frac{\alpha_3^-(k) u_{x_3}^h(k)}{h_3}, & k_3 = N_3. \end{cases}$$

The matrix  $F^h(t)$  is given by

$$(2.24) \quad F^h(k, t) := \begin{cases} f^h(k) + \frac{q(t)}{h_3}, & k_3 = 0, \\ f^h(k), & \text{otherwise.} \end{cases}$$

Before turning to the time discretization of the Cauchy problem (2.21), let us consider some properties of the coefficient matrices as well as the convergence of the solution of (2.21) to the solution of (2.14).

**Lemma 2.9.** *The coefficient matrices  $\mathcal{A}_i, i = 1, 2, 3$ , do not depend on  $t$  and they are positive semi-definite.*

*Proof.* The independence of  $\mathcal{A}_i$  from  $t$  follows directly from the independence of  $\alpha(x)$  from  $t$ . Let us prove that  $\mathcal{A}_1$  is positive semi-definite. The proofs for the other matrices are similar. For an arbitrary three-dimensional matrix  $U := \{U(k), k \in \bar{\Omega}_h\}$ , we have

$$(\mathcal{A}_1 U, U) = \sum_{k_2=0}^{N_2} \sum_{k_3=0}^{N_3} \left( \mathcal{A}_1^{k_2, k_3} U_1(k_2, k_3), U_1(k_2, k_3) \right),$$

where,  
(2.25)

$$\mathcal{A}_1^{k_2, k_3} := \begin{pmatrix} \frac{\alpha_1^+(0, k_2, k_3)}{h_1^2} & -\frac{\alpha_1^+(0, k_2, k_3)}{h_1^2} & \dots & 0 & 0 \\ -\frac{\alpha_1^-(1, k_2, k_3)}{h_1^2} & \frac{2\alpha_1^*(1, k_2, k_3)}{h_1^2} & \dots & 0 & 0 \\ 0 & -\frac{\alpha_1^-(2, k_2, k_3)}{h_1^2} & \dots & 0 & 0 \\ \dots & \dots & \dots & \dots & \dots \\ 0 & 0 & \dots & \frac{2\alpha_1^*(N_1-1, k_2, k_3)}{h_1^2} & -\frac{\alpha_1^+(N_1-1, k_2, k_3)}{h_1^2} \\ 0 & 0 & \dots & -\frac{\alpha_1^-(N_1, k_2, k_3)}{h_1^2} & \frac{\alpha_1^-(N_1, k_2, k_3)}{h_1^2} \end{pmatrix}$$

with  $\alpha_1^*(k) := \frac{1}{2}[\alpha_1^-(k) + \alpha_1^+(k)]$  and

$$U_1(k_2, k_3) := (U(0, k_2, k_3), U(1, k_2, k_3), \dots, U(N_1, k_2, k_3))'.$$

It is noted that  $\alpha_1^+(k) = \alpha_1^-(k + e_1)$ . Hence

$$\left( \mathcal{A}_1^{k_2, k_3} U_1(k_2, k_3), U_1(k_2, k_3) \right) = \sum_{k_1=0}^{N_1-1} \alpha_1^+(k) [U_1(k) - U_1(k + e_1)]^2.$$

It is clear that  $\mathcal{A}_1^{k_2, k_3}$  are positive semi-definite for all  $k_2$  and  $k_3$ , so is  $\mathcal{A}_1$ . □

**Remark 2.10.** From (2.23) we can even prove that matrix  $\mathcal{A}_3$  is positive definite for  $p > 0$ .

**Lemma 2.11.** *Let  $u^h$  be a solution of the Cauchy problem (2.21). Then it is bounded in the norm of  $H^{1,1}(\mathbb{Q}_{ht_e})$ . More precisely,*

$$(2.26) \quad \|u^h\|_{H^{1,1}(\mathbb{Q}_{ht_e})} \leq C,$$

with constant  $C$  independent of  $h$ .

*Proof.* Recall that (2.20) is satisfied for all functions  $\eta$  of which  $\eta(k, \cdot) \in L_2(0, t_e), \forall k \in \bar{\Omega}_h$ . For any  $t^* \in (0, t_e]$ , we set  $\eta(k, t) = u^h(k, t)$  for  $t \in [0, t^*]$  and zero otherwise. Since

$$\int_0^{t^*} dt \sum_{k \in \bar{\Omega}_h} u_t^h(k) u^h(k) = \frac{1}{2} \sum_{k \in \bar{\Omega}_h} [u^h(k, t^*)]^2 - \frac{1}{2} \sum_{k \in \bar{\Omega}_h} [u^h(k, 0)]^2,$$

we have from (2.20) the following equality

$$\begin{aligned} & \frac{1}{2} \Delta h \sum_{k \in \bar{\Omega}_h} [u^h(k, t^*)]^2 + \Delta h \int_0^{t_e} \left\{ \sum_{i=1}^3 \sum_{k \in \bar{\Omega}_i^-} \alpha_i^+(k) [u_{x_i}^h(k)]^2 + \frac{p}{h_3} \sum_{k \in \bar{\Gamma}_h^1} [u^h(k)]^2 \right\} dt \\ &= \frac{1}{2} \Delta h \sum_{k \in \bar{\Omega}_h} [u^h(k, 0)]^2 + \Delta h \int_0^{t_e} dt \sum_{k \in \bar{\Omega}_h} f^h(k) u^h(k) + h_1 h_2 \int_0^{t_e} dt \sum_{k \in \bar{\Gamma}_h^1} q u^h(k). \end{aligned}$$

Multiplying both sides by two, applying Cauchy inequality to the right hand side, we have

$$\begin{aligned} (2.27) \quad & \Delta h \sum_{k \in \bar{\Omega}_h} [u^h(k, t^*)]^2 + 2 \Delta h \int_0^{t_e} \left\{ \sum_{i=1}^3 \sum_{k \in \bar{\Omega}_i^-} \alpha_i^+(k) [u_{x_i}^h(k)]^2 + \frac{p}{h_3} \sum_{k \in \bar{\Gamma}_h^1} [u^h(k)]^2 \right\} dt \\ & \leq \Delta h \sum_{k \in \bar{\Omega}_h} [g^h(k)]^2 + \Delta h \int_0^{t^*} \sum_{k \in \bar{\Omega}_h} [f^h(k, t)]^2 dt + \Delta h \int_0^{t^*} \sum_{k \in \bar{\Omega}_h} [u^h(k, t)]^2 dt \\ & \quad + h_1 h_2 \int_0^{t^*} dt \sum_{k \in \bar{\Gamma}_h^1} \left\{ \frac{1}{\epsilon} q^2(t) + \epsilon [u^h(k)]^2 \right\} \end{aligned}$$

for an arbitrary positive real number  $\epsilon$ . For simplicity of the notation, we denote

$$(2.28) \quad G_1(t^*, \epsilon) := \Delta h \sum_{k \in \bar{\Omega}_h} [g^h(k)]^2 + \Delta h \int_0^{t^*} \sum_{k \in \bar{\Omega}_h} [f^h(k, t)]^2 dt + \frac{h_1 h_2}{\epsilon} \int_0^{t^*} dt \sum_{k \in \bar{\Gamma}_h^1} q^2(t).$$

To eliminate the last term on the right hand side of (2.27), we choose  $\epsilon = 2p$ . Denote

$$y(t^*) := \Delta h \int_0^{t^*} \sum_{k \in \bar{\Omega}_h} [u^h(k, t)]^2 dt.$$

Then from (2.27) and (2.28) we have

$$(2.29) \quad \Delta h \int_0^{t_e} dt \sum_{i=1}^3 \sum_{k \in \bar{\Omega}_i^-} [u_{x_i}^h(k)]^2 \leq \frac{1}{2\nu} G_1(t_e, 2p) + \frac{1}{2\nu} y(t_e)$$

and

$$y'(t^*) \leq G_1(t^*, 2p) + y(t^*).$$

Applying Gronwall-Bellman's lemma [18] to this inequality, we obtain

$$(2.30) \quad y(t^*) \leq (e^{t^*} - 1) G_1(t^*, 2p).$$

In order to obtain a bound estimate for  $\Delta h \int_0^{t_e} dt \sum_{k \in \bar{\Omega}_h} [u_t^h(k)]^2$ , we replace  $\eta^h$  in (2.20) by  $u_t^h$ . We have

$$(2.31) \quad \begin{aligned} & \Delta h \int_0^{t_e} dt \left\{ \sum_{k \in \bar{\Omega}_h} [u_t^h(k)]^2 + \sum_{i=1}^3 \sum_{k \in \bar{\Omega}_i^-} \alpha_i^+(k) u_{x_i}^h(k) u_{x_i t}^h(k) + \frac{p}{h_3} \sum_{k \in \bar{\Gamma}_h^1} u^h(k) u_t^h(k) \right\} \\ &= \Delta h \int_0^{t_e} dt \sum_{k \in \bar{\Omega}_h} f^h(k) u_t^h(k) + h_1 h_2 \int_0^{t_e} dt \sum_{k \in \bar{\Gamma}_h^1} q(t) u_t^h(k). \end{aligned}$$

Multiplying both sides by two, integrating the second and the third terms on the left hand side, integrating by parts the right hand side, we obtain

$$\begin{aligned} & 2\Delta h \int_0^{t_e} dt \sum_{k \in \bar{\Omega}_h} [u_t^h(k)]^2 + \Delta h \sum_{i=1}^3 \sum_{k \in \bar{\Omega}_i^-} \alpha_i^+(k) \left\{ [u_{x_i}^h(k, t_e)]^2 - [u_{x_i}^h(k, 0)]^2 \right\} \\ &+ h_1 h_2 p \sum_{k \in \bar{\Gamma}_h^1} \left\{ [u^h(k, t_e)]^2 - [u^h(k, 0)]^2 \right\} = 2\Delta h \int_0^{t_e} dt \sum_{k \in \bar{\Omega}_h} f^h(k) u_t^h(k) \\ &+ 2h_1 h_2 \sum_{k \in \bar{\Gamma}_h^1} \left[ q(t_e) u^h(k, t_e) - q(0) u^h(k, 0) - \int_0^{t_e} q_t(t) u^h(k) dt \right]. \end{aligned}$$

Transposing the terms on the left hand side with minus sign to the right hand side, applying Cauchy's inequality to the right hand side, taking into account the

assumption that  $\nu \leq \alpha(x) \leq \mu$ , we have

$$\begin{aligned}
 (2.32) \quad & 2\Delta h \int_0^{t_e} dt \sum_{k \in \bar{\Omega}_h} [u_t^h(k)]^2 + \Delta h \sum_{i=1}^3 \sum_{k \in \bar{\Omega}_i^-} \alpha_i^+(k) [u_{x_i}^h(k, t_e)]^2 + h_1 h_2 p \sum_{k \in \bar{\Gamma}_h^1} [u^h(k, t_e)]^2 \\
 & \leq \Delta h \mu \sum_{i=1}^3 \sum_{k \in \bar{\Omega}_i^-} [g_{x_i}^h(k)]^2 + h_1 h_2 \mu p \sum_{k \in \bar{\Gamma}_h^1} [g^h(k)]^2 + \Delta h \int_0^{t_e} dt \sum_{k \in \bar{\Omega}_h} [f^h(k)]^2 \\
 & + \Delta h \int_0^{t_e} dt \sum_{k \in \bar{\Omega}_h} [u_t^h(k)]^2 + \frac{h_1 h_2}{\epsilon} \sum_{k \in \bar{\Gamma}_h^1} q^2(t_e) + \epsilon h_1 h_2 \sum_{k \in \bar{\Gamma}_h^1} [u^h(k, t_e)]^2 \\
 & + h_1 h_2 \sum_{k \in \bar{\Gamma}_h^1} q^2(0) + h_1 h_2 \sum_{k \in \bar{\Gamma}_h^1} [g^h(k)]^2 + h_1 h_2 \int_0^{t_e} dt \sum_{k \in \bar{\Gamma}_h^1} \left\{ \frac{1}{h_3} q_t^2(t) + h_3 [u^h(k)]^2 \right\}.
 \end{aligned}$$

Choose  $\epsilon = p$ , then the last term on the left hand side is eliminated by the same term on the right hand side. The fourth term on the right hand side is also eliminated by the first term on the left hand side. For abbreviating the notation, we denote

$$\begin{aligned}
 (2.33) \quad G_2 := & \Delta h \mu \sum_{i=1}^3 \sum_{k \in \bar{\Omega}_i^-} [g_{x_i}^h(k)]^2 + h_1 h_2 (\mu p + 1) \sum_{k \in \bar{\Gamma}_h^1} [g^h(k)]^2 + \Delta h \int_0^{t_e} dt \sum_{k \in \bar{\Omega}_h} [f^h(k)]^2 \\
 & + \frac{h_1 h_2}{p} \sum_{k \in \bar{\Gamma}_h^1} q^2(t_e) + h_1 h_2 \sum_{k \in \bar{\Gamma}_h^1} q^2(0) + \frac{h_1 h_2}{h_3} \int_0^{t_e} dt \sum_{k \in \bar{\Gamma}_h^1} q_t^2(t).
 \end{aligned}$$

It follows from (2.32) and (2.33) that

$$\begin{aligned}
 (2.34) \quad \Delta h \int_0^{t_e} dt \sum_{k \in \bar{\Omega}_h} [u_t^h(k)]^2 & \leq G_2 + \Delta h \int_0^{t_e} dt \sum_{k \in \bar{\Gamma}_h^1} [u^h(k)]^2 \\
 & \leq G_2 + y(t_e).
 \end{aligned}$$

From (2.29), (2.30) and (2.34) we have

$$\|u^h\|_{H^{1,1}(\mathbb{Q}_{ht_e})}^2 \leq G_2 + \frac{(4\nu + 1)(e^{t_e} - 1) + 1}{2\nu} G_1(t_e, 2p).$$

It can be proved from (2.28) that there exists a positive constant  $C^*$  such that

$$G_1(t_e, 2p) \leq C^* \left[ \|g\|_{L_2(\Omega)}^2 + \|f\|_{L_2(\mathbb{Q}_{t_e})}^2 + \|q\|_{L_2(0,t_e)}^2 \right].$$

A similar estimate can be obtained for  $G_2$ . Hence, we have proved that the grid function  $u^h$  is bounded in the norm of  $H^{1,1}(\mathbb{Q}_{ht_e})$ .  $\square$

**Remark 2.12.** It follows from Lemmas 2.9 and 2.11 that there is only one solution of the Cauchy problem (2.21).

From Lemma 2.11 we have the convergence of the solution  $u^h(k, t)$  of (2.21) to the solution of the original problem. We state this property in the following theorem.

**Theorem 2.13.** *The multi-linear interpolation (2.18) of the solution of the problem (2.21) on  $\mathbb{Q}_{t_e}$  converges to the generalized solution of the original problem (2.14) strongly in the norm of  $L_2(\mathbb{Q}_{t_e})$  and weakly in the norm of  $H^{1,1}(\mathbb{Q}_{t_e})$  as the grid size  $h$  tends to zero.*

*Proof.* It follows from Lemmas 2.6 and 2.11 that the sequence  $\{\hat{u}^h\}_h$  of the multi-linear interpolations is bounded in  $H^{1,1}(\mathbb{Q}_{t_e})$ . It follows from the compact imbedding theorem of Sobolev spaces (see, e.g. [18]) that it is weakly relatively compact in  $H^{1,1}(\mathbb{Q}_{t_e})$  and strongly relatively compact in  $L_2(\mathbb{Q}_{t_e})$ . Hence, there is a subsequence  $\{\hat{u}^{h^i}(x, t)\}_i$  such that it converges strongly to a function  $u(x, t)$  and the sequence of the derivative  $\{\hat{u}_{x_j}^{h^i}(x, t)\}_i$  converges weakly to the corresponding derivative  $u_{x_j}(x, t)$  in the norm of  $L_2(\mathbb{Q}_{t_e})$  as  $i$  tends to infinity (equivalently,  $h^i$  tends to zero) for  $j = 1, 2, 3$ . Therefore  $u(x, t) \in H^{1,1}(\mathbb{Q}_{t_e})$ .

From Lemmas 2.7 and 2.8 it follows that the corresponding sequence of piecewise constant interpolations  $\{\tilde{u}^{h^i}(x, t)\}_i$  also converges to  $u(x, t)$  in the same manner. To finish the proof, we need to show that each term in the discrete equation (2.20) converges to the corresponding one in (2.14). Indeed, since  $C^{2,1}(\mathbb{Q}_{t_e})$  is dense in  $H^{1,1}(\mathbb{Q}_{t_e})$ , it is enough to consider the function  $\eta$  in this space. The values of the grid function  $\eta^h$  in (2.20) are set to be the values of  $\eta$  at the grid points. It is clear that  $\eta^h$  converges uniformly to  $\eta$  as  $h$  tends to zero. This implies that all the terms in (2.20) also converge to the corresponding terms in (2.14). That means,  $u$  is a generalized solution of the original problem. Hence, the uniqueness theorem implies that every subsequence of  $\{\hat{u}^h(x, t)\}_h$  converges to the same function  $u$ . So the sequence  $\{\hat{u}^h(x, t)\}_h$  itself converges to  $u$ . This completes the proof.  $\square$

**2.3.3. Time discretization and implicit splitting scheme.** Solving the problem (2.21) is usually time-consuming. To reduce the computation cost, we make use of splitting methods. The main idea of these methods is to replace a complicated problem by a chain of simpler ones. The methods were initiated by Douglas, Peaceman and Rachford [10, 25] and then developed by Bagrinovskii, Godunov, Yanenko, Samarskii [26, 30, 27, 28], Dyakonov, Saulyev, and Marchuk [22, 21]. These methods have many advantages for solving multi-dimensional problems. For example, they are absolutely stable and much faster than implicit schemes as it does not require iterative procedures for solving large linear systems.

To discretize (2.21), we divide the interval  $[0, t_e]$  into  $N_t$  equal sub-intervals by the points  $t_i$ ,  $i = 0, \dots, N_t$ :  $0 = t_0 < t_1 = \Delta t < t_2 = 2\Delta t < \dots < t_{N_t} = t_e$ . We set  $u^{n+\epsilon} = u^h(t_n + \epsilon\Delta t)$  and  $F^{n+\epsilon} = F^h(t_n + \epsilon\Delta t)$  with  $0 \leq \epsilon \leq 1$  (we drop the

superscript  $h$  for simplifying the notation). We introduce the following backward implicit splitting scheme

$$(2.35) \quad \begin{cases} u^0 = g^h, \\ (E_1 + \Delta t \mathcal{A}_1)u^{n+\frac{1}{3}} = u^n, \\ (E_2 + \Delta t \mathcal{A}_2)u^{n+\frac{2}{3}} = u^{n+\frac{1}{3}}, \\ (E_3 + \Delta t \mathcal{A}_3)u^{n+1} = u^{n+\frac{2}{3}} + \Delta t F^{n+\frac{1}{2}}, \end{cases}$$

for  $n = 0, \dots, N_t - 1$ . Here  $E_i$  is the unit matrix associated with  $\mathcal{A}_i$ ,  $i = 1, 2, 3$ . Since the coefficient matrices are positive semi-definite as proven in Lemma 2.9, the above splitting scheme is absolutely stable and converges to the solution of problem (2.21) with the first order in  $t$  ([21], pages 167–168).

### 3. INVERSE PROBLEM FOR LANDMINE DETECTION

Given the forward thermal model (2.12) and IR images measured at the air-soil interface, we now consider the inverse problem for landmine detection. We should note that the measured IR images can be considered as measured soil temperature at the air-soil interface. The purpose of this problem is to detect the presence of buried objects and characterize them based on the estimation of their thermal as well as geometrical parameters. Mathematically, it is stated as the reconstruction of the coefficient  $\alpha(x)$ ,  $x \in \Omega$ , of the forward thermal model (2.12) from the measurements of the solution to the forward model,  $T(x, t)$ , for  $(x, t) \in S_{t_e}^1$ .

The most common way to set up this inverse problem is the least-squares approach in which the estimation problem is aimed at finding  $\alpha(x)$  such that the simulated soil-surface temperature using the forward model (2.12) fits the measured data. It is equivalent to the following minimization problem

$$(3.1) \quad \min_{\alpha(x)} \mathcal{F}(\alpha) := \frac{1}{2} \int_{S_{t_e}^1} [T(x, t; \alpha) - \theta(x, t)]^2 dx'_3 dt,$$

where  $\theta(x, t)$  is the measured soil-surface temperature (IR images). Here we use the notation  $T(x, t; \alpha)$  to emphasize the dependence of the solution to the forward problem (2.12) on the coefficient  $\alpha(x)$ .

We note that, since thermal properties of materials are positive and finite, the following bound constraints must be taken into account in solving the inverse problem (3.1) subject to (2.12)

$$(3.2) \quad 0 < \alpha^l \leq \alpha(x) \leq \alpha^u, \quad x \in \Omega,$$

where  $[\alpha^l, \alpha^u]$  is the range to which the thermal diffusivity of the object is expected to belong.

**Remark 3.1.** Although some results on the uniqueness of the coefficient identification problem have been published in the literature, most of the published works requires more than one (even infinitely many) measurements on the whole boundary or even in the whole domain for the coefficient to be uniquely determined,

see, e.g., [11, 12, 13, 14]. The uniqueness for a one-dimensional coefficient estimation problem with one measurement taken at one end of the one-dimensional rod has been proved by Dinh Nho Hào [7]. Recently, such a result for piecewise constant coefficients was reproved by Hoang and Ramm [15] by another method. However, the techniques used in these papers cannot be generalized to multidimensional cases. Moreover, for this problem, the main difficulty is due to the lack of spatial data as we want to determine the three-dimensional coefficient when only one measurement on a part of the boundary is given. Therefore, the uniqueness question is still open to us. For some simple cases, the analysis is under investigation.

The existence of a solution to problem (3.1) was proved in [31] in the space  $BV(\Omega)$  of functions with bounded variation.

**3.1. Discrete inverse problem and the gradient of the objective functional.** To numerically solve the minimization problem (3.1) subject to (2.12), we make use gradient-based optimization algorithms. More precisely, we use the Matlab function *fmincon* which implements a quasi-Newton trust region algorithm, see [23]. In gradient-based optimization methods, it is required to calculate the gradient of the objective functional. In this paper, we use the method of adjoint problems for this purpose. This technique helps calculating the gradient of the objective functional by solving one forward and one adjoint problem. Moreover, to avoid discretization errors in numerical implementation, we apply this method directly to the discretized problem. That is, we first formulate the discrete objective functional corresponding to the discrete forward model (2.35), with  $u$  being replaced by  $T$ . Then the gradient of the discrete objective functional is calculated. This approach was also used in [33].

In this discrete setup, the objective functional  $\mathcal{F}(\alpha)$  of minimization problem (3.1) is replaced by the following discrete one:

$$(3.3) \quad \mathcal{F}_h(\alpha) := \frac{\Delta t h_1 h_2}{2} \sum_{n=0}^{N_t} \sum_{k \in \bar{\Gamma}_h^1} [T^n(k; \alpha) - \theta^n(k_1, k_2)]^2,$$

with  $\{T^n(k; \alpha), k \in \bar{\Omega}_h, n = 0, \dots, N_t\}$  being the solution of the discrete forward problem (2.35) associated with the coefficient  $\alpha(x)$  and  $\{\theta^n(k_1, k_2), 0 \leq k_i \leq N_i, n = 0, \dots, N_t\}$  being the discrete measured soil-surface temperature. It is clear that the discrete objective functional  $\mathcal{F}_h(\alpha)$  is an approximation of the continuous one.

It should be noted that, in the discrete problem, the coefficient  $\alpha(x)$ ,  $x \in \Omega$ , can be replaced by the average values  $\alpha_i^+(k)$ . For shortening the notation, in the following, we denote  $\alpha_i(k) := \alpha_i^+(k)$  and  $\alpha_i := \{\alpha_i(k), k \in \bar{\Omega}_i^-\}$ . Since  $\alpha(x)$  is bounded by (3.2), the average values  $\alpha_i(k)$  are also bounded by

$$(3.4) \quad 0 < \alpha^l \leq \alpha_i(k) \leq \alpha^u, \quad k \in \bar{\Omega}_i^-, \quad i \in \{1, 2, 3\}.$$

For each  $i = 1, 2, 3$  it is clear from (2.22)–(2.23) that the coefficient matrix  $\mathcal{A}_i$  depends on (and only on)  $\alpha_i$  (in the following, we sometimes use the notation  $\mathcal{A}_i(\alpha_i)$  to emphasize the dependence of  $\mathcal{A}_i$  on  $\alpha_i$ ). Moreover, with the assumption

that the object is so small that the vertical boundary layers of the soil domain contain only homogeneous soil, we have that  $\alpha_i(k) = \alpha_s$  at the vertical boundary points, e.g. for  $k_1 = 0$  or  $k_1 = N_1$ . Hence, we only need to consider the variables  $\alpha_i(k)$  for  $1 \leq k_1 \leq N_1 - 1$ ,  $1 \leq k_2 \leq N_2 - 1$ ,  $0 \leq k_3 \leq N_3 - 1$ . This assumption helps reducing the complexity of the numerical implementation.

We also note that the discrete forward model (2.35), with  $u$  being replaced by  $T$ , can be rewritten as

$$(3.5) \quad \begin{cases} \mathcal{A}(\alpha)T^{n+1} - T^n = \Delta t \mathcal{C}(\alpha)F^{n+\frac{1}{2}}, & n = 0, \dots, N_t - 1, \\ T^0 = g^h, \end{cases}$$

where

$$\begin{aligned} \mathcal{A}(\alpha) &= (E_1 + \Delta t \mathcal{A}_1(\alpha_1)) (E_2 + \Delta t \mathcal{A}_2(\alpha_2)) (E_3 + \Delta t \mathcal{A}_3(\alpha_3)), \\ \mathcal{C}(\alpha) &= (E_1 + \Delta t \mathcal{A}_1(\alpha_1)) (E_2 + \Delta t \mathcal{A}_2(\alpha_2)). \end{aligned}$$

Let us now formulate the gradient of the discrete objective functional  $\mathcal{F}_h$  with respect to the unknowns  $\alpha_i$ . To this end, we consider an infinitesimal variation  $\delta\alpha$  of the coefficient  $\alpha$ . By denoting  $\alpha'(x) = \alpha(x) + \delta\alpha(x)$  and  $\alpha'_i(k) = \alpha_i(k) + \delta\alpha_i(k)$ , we have from (3.3) that

$$(3.6) \quad \begin{aligned} \mathcal{F}_h(\alpha') - \mathcal{F}_h(\alpha) &= \frac{\Delta t h_1 h_2}{2} \sum_{n=0}^{N_t} \sum_{k_1=0}^{N_1} \sum_{k_2=0}^{N_2} [T^n(k_1, k_2, 0; \alpha') - \theta^n(k_1, k_2)]^2 \\ &\quad - \frac{\Delta t h_1 h_2}{2} \sum_{n=0}^{N_t} \sum_{k_1=0}^{N_1} \sum_{k_2=0}^{N_2} [T^n(k_1, k_2, 0; \alpha) - \theta^n(k_1, k_2)]^2 \\ &= \frac{\Delta t h_1 h_2}{2} \sum_{n=0}^{N_t} \sum_{k_1=0}^{N_1} \sum_{k_2=0}^{N_2} [U^n(k_1, k_2, 0)]^2 \\ &\quad + \Delta t h_1 h_2 \sum_{n=0}^{N_t} \sum_{k_1=0}^{N_1} \sum_{k_2=0}^{N_2} U^n(k_1, k_2, 0) [T^n(k_1, k_2, 0; \alpha) - \theta^n(k_1, k_2)], \end{aligned}$$

where  $U^n(k) := T^n(k; \alpha') - T^n(k; \alpha)$ . It follows from (3.5) that  $U := \{U^n(k), n = 0, \dots, N_t - 1, k \in \bar{\Omega}_h\}$  is the solution of the following problem

$$\begin{cases} [\mathcal{A}(\alpha)U^{n+1}] (k) - U^n(k) = \Delta t \left[ \delta \mathcal{C}(\alpha)F^{n+\frac{1}{2}} \right] (k) - [\delta \mathcal{A}(\alpha)T^{n+1}] (k, \alpha'), \\ U^0 = 0, \end{cases} \quad n = 0, \dots, N_t - 1,$$

where  $\delta \mathcal{C}(\alpha) = \mathcal{C}(\alpha') - \mathcal{C}(\alpha)$  and  $\delta \mathcal{A}(\alpha) = \mathcal{A}(\alpha') - \mathcal{A}(\alpha)$ . Consider an arbitrary matrix  $\eta = \{\eta^n(k), n = 0, \dots, N_t - 1, k \in \bar{\Omega}_h\}$ . Multiplying both sides of the first equation by  $\eta^n(k)$ , summing up the results with respect to  $k \in \bar{\Omega}_h$  and

$n = 0, \dots, N_t - 1$ , we have

$$\begin{aligned} & \sum_{n=0}^{N_t-1} \sum_{k \in \bar{\Omega}_h} [\mathcal{A}(\alpha)U^{n+1}](k)\eta^{n+1}(k) - \sum_{n=0}^{N_t-1} \sum_{k \in \bar{\Omega}_h} U^n(k)\eta^{n+1}(k) \\ &= \Delta t \sum_{n=0}^{N_t-1} \sum_{k \in \bar{\Omega}_h} \left[ \delta \mathcal{C}(\alpha)F^{n+\frac{1}{2}} \right](k)\eta^{n+1}(k) - \sum_{n=0}^{N_t-1} \sum_{k \in \bar{\Omega}_h} [\delta \mathcal{A}(\alpha)T^{n+1}](k, \alpha')\eta^{n+1}(k). \end{aligned}$$

If  $\eta$  satisfies the following equation

$$\begin{aligned} (3.7) \quad & \sum_{n=0}^{N_t-1} \sum_{k \in \bar{\Omega}_h} [\mathcal{A}(\alpha)U^{n+1}](k)\eta^{n+1}(k) - \sum_{n=0}^{N_t-1} \sum_{k \in \bar{\Omega}_h} U^n(k)\eta^{n+1}(k) \\ &= \frac{1}{h_3} \sum_{n=0}^{N_t} \sum_{k_1=0}^{N_1} \sum_{k_2=0}^{N_2} U^n(k_1, k_2, 0) [T^n(k_1, k_2, 0; \alpha) - \theta^n(k_1, k_2)], \end{aligned}$$

then the variation of the discrete objective functional is given by

$$\begin{aligned} (3.8) \quad \mathcal{F}_h(\alpha') - \mathcal{F}_h(\alpha) &= \frac{\Delta t h_1 h_2}{2} \sum_{n=0}^{N_t} \sum_{k_1=0}^{N_1} \sum_{k_2=0}^{N_2} [U^n(k_1, k_2, 0)]^2 \\ &+ \Delta t^2 \Delta h \sum_{n=0}^{N_t-1} \sum_{k \in \bar{\Omega}_h} \left[ \delta \mathcal{C}(\alpha)F^{n+\frac{1}{2}} \right](k)\eta^{n+1}(k) \\ &- \Delta t \Delta h \sum_{n=0}^{N_t-1} \sum_{k \in \bar{\Omega}_h} [\delta \mathcal{A}(\alpha)T^{n+1}](k, \alpha')\eta^{n+1}(k). \end{aligned}$$

Before deriving the gradient of  $\mathcal{F}_h(\alpha)$ , let us first define the discrete adjoint problem from (3.7). Suppose that  $\xi = \{\xi^n(k), k \in \bar{\Omega}_h, n = 0, \dots, N_t\}$  is specified by

$$(3.9) \quad \xi^n(k) = \begin{cases} \frac{1}{h_3} [T^n(k; \alpha) - \theta^n(k_1, k_2)] & \text{if } k_3 = 0, \\ 0 & \text{otherwise,} \end{cases}$$

then we have from (3.7) the following discrete adjoint problem

$$(3.10) \quad \begin{cases} \mathcal{A}^*(\alpha)\eta^n - \eta^{n+1} = \xi^n, & n = N_t - 1, N_t - 2, \dots, 2, \\ \mathcal{A}^*(\alpha)\eta^{N_t} = \xi^{N_t}, \end{cases}$$

with  $\mathcal{A}^*(\alpha)$  being the adjoint operator of  $\mathcal{A}(\alpha)$ . Since the matrices  $A_i, i = 1, 2, 3$ , are positive semi-definite and symmetric as proved in Section 2, we have

$$A^*(\alpha) = (E_3 + \Delta t A_3)(E_2 + \Delta t A_2)(E_1 + \Delta t A_1).$$

With the above representation of the operator  $\mathcal{A}^*(\alpha)$ , the discrete adjoint problem can be rewritten in the following form

- For  $n = N_t$  :

$$\begin{cases} (E_3 + \Delta t \mathcal{A}_3) \eta^{N_t + \frac{2}{3}} = \xi^{N_t}, \\ (E_2 + \Delta t \mathcal{A}_2) \eta^{N_t + \frac{1}{3}} = \eta^{N_t + \frac{2}{3}}, \\ (E_1 + \Delta t \mathcal{A}_1) \eta^{N_t} = \eta^{N_t + \frac{1}{3}}. \end{cases}$$

- For  $n = N_t - 1, N_t - 2, \dots, 2$  :

$$\begin{cases} (E_3 + \Delta t \mathcal{A}_3) \eta^{n + \frac{2}{3}} = \xi^n + \eta^{n+1}, \\ (E_2 + \Delta t \mathcal{A}_2) \eta^{n + \frac{1}{3}} = \eta^{n + \frac{2}{3}}, \\ (E_1 + \Delta t \mathcal{A}_1) \eta^n = \eta^{n + \frac{1}{3}}. \end{cases}$$

This problem is solved in a similar way as the discrete forward model (2.35).

We now turn back to the gradient of the discrete objective functional. We can prove by induction that [31]

$$(3.11) \quad \frac{\Delta t h_1 h_2}{2} \sum_{n=0}^{N_t} \sum_{k_1=0}^{N_1} \sum_{k_2=0}^{N_2} [U^n(k_1, k_2, 0)]^2 = o(\delta\alpha).$$

We also have

$$\begin{aligned} \delta\mathcal{C}(\alpha) &= [E_1 + \Delta t \mathcal{A}_1(\alpha'_1)][E_2 + \Delta t \mathcal{A}_2(\alpha'_2)] - [E_1 + \Delta t \mathcal{A}_1(\alpha_1)][E_2 + \Delta t \mathcal{A}_2(\alpha_2)] \\ &= \Delta t \delta \mathcal{A}_1(\alpha_1)[E_2 + \Delta t \mathcal{A}_2(\alpha'_2)] + \Delta t [E_1 + \Delta t \mathcal{A}_1(\alpha_1)] \delta \mathcal{A}_2(\alpha_2), \end{aligned}$$

with  $\delta \mathcal{A}_i(\alpha_i) = \mathcal{A}_i(\alpha'_i) - \mathcal{A}_i(\alpha_i)$ . We note that  $F^{n+\frac{1}{2}}(k)$  does not depend on either the coefficient  $\alpha(x)$  or the values of  $k_1$  and  $k_2$ . Therefore,  $\mathcal{A}_1 F^{n+\frac{1}{2}}(k) = 0$  and  $\mathcal{A}_2 F^{n+\frac{1}{2}}(k) = 0$  for  $k \in \bar{\Omega}_h$ . By elementary arguments, we also have that  $\delta C(\alpha) F^{n+\frac{1}{2}} = 0$ . From these equalities, (3.8) and (3.11), the variation of the objective functional can be rewritten as

$$(3.12) \quad \mathcal{F}_h(\alpha') - \mathcal{F}_h(\alpha) = -\Delta t \Delta h \sum_{n=1}^{N_t} \sum_{k \in \bar{\Omega}_h} (\delta \mathcal{A}(\alpha) T^n)(k, \alpha') \eta^n(k) + o(\delta\alpha).$$

The variation  $\delta \mathcal{A}(\alpha)$  can be represented by

$$\delta \mathcal{A}(\alpha) = \delta \mathcal{A}^1(\alpha) + \delta \mathcal{A}^2(\alpha) + \delta \mathcal{A}^3(\alpha),$$

where

$$\begin{aligned} \delta \mathcal{A}^1(\alpha) &= \Delta t \delta \mathcal{A}_1(\alpha_1) [E_2 + \Delta t \mathcal{A}_2(\alpha'_2)] [E_3 + \Delta t \mathcal{A}_3(\alpha'_3)], \\ \delta \mathcal{A}^2(\alpha) &= \Delta t [E_1 + \Delta t \mathcal{A}_1(\alpha_1)] \delta \mathcal{A}_2(\alpha_2) [E_3 + \Delta t \mathcal{A}_3(\alpha'_3)], \\ \delta \mathcal{A}^3(\alpha) &= \Delta t [E_1 + \Delta t \mathcal{A}_1(\alpha_1)] [E_2 + \Delta t \mathcal{A}_2(\alpha_2)] \delta \mathcal{A}_3(\alpha_3). \end{aligned}$$

From (2.22)–(2.23) we have that for each  $i \in \{1, 2, 3\}$ , the coefficient matrix  $\mathcal{A}_i$  is continuous in  $\alpha_i$ . Therefore,  $\mathcal{A}_i(\alpha'_i)$  converges to  $\mathcal{A}_i(\alpha_i)$  as  $\delta\alpha$  tends to zero. To derive the gradient of the objective functional, it is sufficient to formulate the

directional derivatives of  $\mathcal{A}_i(\alpha_i)T^n$  with respect to  $\alpha_i(k)$ . For  $k \in \bar{\Omega}_h : 1 \leq k_1 \leq N_1 - 1$ , we have

$$\begin{aligned} [\delta \mathcal{A}^1(\alpha)T^n](k) &= \frac{\Delta t}{h_1} ([E_2 + \Delta t \mathcal{A}_2(\alpha'_2)][E_3 + \Delta t \mathcal{A}_3(\alpha'_3)]T^n)_{\bar{x}_1}(k) \delta \alpha_1(k - e_1) \\ &\quad - \frac{\Delta t}{h_1} ([E_2 + \Delta t \mathcal{A}_2(\alpha'_2)][E_3 + \Delta t \mathcal{A}_3(\alpha'_3)]T^n)_{x_1}(k) \delta \alpha_1(k). \end{aligned}$$

Therefore,  
(3.13)

$$\frac{\partial [\mathcal{A}^1(\alpha_1)T^n](m)}{\partial \alpha_1(k)} = \begin{cases} -\frac{\Delta t}{h_1} ([E_2 + \Delta t \mathcal{A}_2(\alpha'_2)][E_3 + \Delta t \mathcal{A}_3(\alpha'_3)]T^n)_{x_1}(k) & \text{if } m = k, \\ \frac{\Delta t}{h_1} ([E_2 + \Delta t \mathcal{A}_2(\alpha'_2)][E_3 + \Delta t \mathcal{A}_3(\alpha'_3)]T^n)_{x_1}(k) & \text{if } m = k + e_1, \\ 0 & \text{otherwise.} \end{cases}$$

Since  $\mathcal{A}_2$  and  $\mathcal{A}_3$  do not depend on  $\alpha_1$ , taking the limit as  $\delta \alpha_1$  tends to zero, we have from (3.12) and (3.13) that

$$\begin{aligned} (3.14) \quad \frac{\partial \mathcal{F}_h}{\partial \alpha_1(k)} &= -\Delta t \Delta h \sum_{n=1}^{N_t} \sum_{m \in \bar{\Omega}_h} \frac{\partial [(\mathcal{A}^1 T^n)(m)]}{\partial \alpha_1(k)} \eta^n(m) \\ &= -\Delta t \Delta h \sum_{n=1}^{N_t} \left\{ \frac{\partial [(\mathcal{A}^1 T^n)(k)]}{\partial \alpha_1(k)} \eta^n(k) + \frac{\partial [(\mathcal{A}^1 T^n)(k + e_1)]}{\partial \alpha_1(k)} \eta^n(k + e_1) \right\} \\ &= -\Delta t^2 \Delta h \sum_{n=1}^{N_t} [(E_2 + \Delta t \mathcal{A}_2)(E_3 + \Delta t \mathcal{A}_3)T^n]_{x_1}(k) \eta^n(k). \end{aligned}$$

Denoting  $\mu_i = \Delta t/h_i^2$ ,  $i = 1, 2, 3$ , we obtain, for  $1 \leq k_2 \leq N_2 - 1$ ,  $1 \leq k_3 \leq N_3 - 1$ ,

$$\begin{aligned} (3.15) \quad [(E_2 + \Delta t \mathcal{A}_2)(E_3 + \Delta t \mathcal{A}_3)T^n](k) &= \\ &= -\mu_2 \alpha_2(k - e_2) [T^n(k - e_2) + \mu_3 \alpha_3(k - e_2 - e_3) h_3 T^n_{\bar{x}_3}(k - e_2) - \mu_3 \alpha_3(k - e_2) h_3 T^n_{x_3}(k - e_2)] \\ &\quad + [1 + \mu_2(\alpha_2(k - e_2) + \alpha_2(k))] [T^n(k) + \mu_3 \alpha_3(k - e_3) h_3 T^n_{\bar{x}_3}(k) - \mu_3 \alpha_3(k) h_3 T^n_{x_3}(k)] \\ &\quad - \mu_2 \alpha_2(k) [T^n(k + e_2) + \mu_3 \alpha_3(k + e_2 - e_3) h_3 T^n_{\bar{x}_3}(k + e_2) - \mu_3 \alpha_3(k + e_2) h_3 T^n_{x_3}(k + e_2)]. \end{aligned}$$

Similarly, for  $1 \leq k_2 \leq N_2 - 1$ ,  $k_3 = 0$ , we have

$$\begin{aligned} (3.16) \quad [(E_2 + \Delta t \mathcal{A}_2)(E_3 + \Delta t \mathcal{A}_3)T^n](k) &= \\ &= -\mu_2 \alpha_2(k - e_2) \{ (1 + \mu_3 p h_3) T^n(k - e_2) - \mu_3 \alpha_3(k - e_2) [T^n(k - e_2 + e_3) - T^n(k - e_2)] \} \\ &\quad + [1 + \mu_2(\alpha_2(k - e_2) + \alpha_2(k))] \{ (1 + \mu_3 p h_3) T^n(k) - \mu_3 \alpha_3(k) [T^n(k + e_3) - T^n(k)] \} \\ &\quad - \mu_2 \alpha_2(k) \{ (1 + \mu_3 p h_3) T^n(k + e_2) - \mu_3 \alpha_3(k + e_2) [T^n(k + e_2 + e_3) - T^n(k + e_2)] \}. \end{aligned}$$

The directional derivatives of the objective functional with respect to  $\alpha_1(k)$ ,  $1 \leq k_1 \leq N_1 - 1$ ,  $1 \leq k_2 \leq N_2 - 1$ ,  $0 \leq k_3 \leq N_3 - 1$ , are calculated using (3.14)–(3.16). The derivatives of  $\mathcal{F}_h$  with respect to  $\alpha_2(k)$  and  $\alpha_3(k)$  are given by similar formulae, see also [31].

**3.2. Parameterization of landmine shape.** The inverse problem (3.3) subject to (3.5) for estimating the coefficient  $\alpha(x)$  is severely ill-posed due to the lack of spatial information in the measured data. Numerical tests have indicated that it is difficult to obtain reliable estimates unless more constraints or simplifications must be used. The constraints or simplifications are based on particular applications. As our objective is to detect landmines and distinguish them from other objects, we assume that landmines are upright cylinders. Under this assumption, a buried object is specified by (i) its depth of burial, (ii) its height, (iii) its horizontal cross-section, and (iv) its thermal diffusivity.

In [31, 35, 33] we proposed a two-step method for solving the inverse problem. In the first step, we considered a given cross-section, and we estimate three parameters, namely, the depth of burial, the height, and the thermal diffusivity. This approach helps reducing the ill-posedness of the estimation problem as it reduces the number of unknown parameters. However, its result depends on the accuracy of the cross-section being given by anomaly detection procedures. In the second step, we used the result of the previous step as an initial guess for estimating the full parameter vector, namely, the depth of burial, the height and the mean values of the thermal diffusivity on a horizontal plane of the soil domain across the object. The cross-section is improved via the estimated mean values of the thermal diffusivity. This step should enhance the result of the first step.

To parametrize the object's shape, we denote by  $\tilde{\Gamma}^1$  its cross-section,  $\varrho_1$  and  $\varrho_2$  are the depths of the top and the bottom surfaces ( $0 < \varrho_1 < \varrho_2 < l_3$ ). Then the coefficient  $\alpha$  can be written as

$$(3.17) \quad \alpha(x) = \begin{cases} \alpha_o, & \text{for } (x_1, x_2) \in \tilde{\Gamma}^1, \varrho_1 \leq x_3 \leq \varrho_2, \\ \alpha_s, & \text{otherwise.} \end{cases}$$

We assume further that the cross-section of the buried object is star-shaped. In this case, the boundary of the cross-section  $\partial\tilde{\Gamma}^1$  in  $\mathbb{R}^2$  can be represented by

$$(3.18) \quad \partial\tilde{\Gamma}^1 := \{(x_1^0, x_2^0)' + r(\varphi)(\cos \varphi, \sin \varphi)', \varphi \in [0, 2\pi]\},$$

where  $(x_1^0, x_2^0)'$  is a given internal point of the cross section in the horizontal plane and the radial function  $r$  is positive in  $[0, 2\pi]$  with  $r(0) = r(2\pi)$ . Note that the point  $(x_1^0, x_2^0)'$  is not difficult to find from the measured IR images. Since the radial function  $r(\varphi)$  satisfies  $r(0) = r(2\pi)$ , it can be considered as a periodic function with the period of  $2\pi$ . Hence, we can represent it as the following Fourier series

$$(3.19) \quad r(\varphi) = \beta_0 + \sum_{m=1}^{\infty} (\beta_m \cos m\varphi + \gamma_m \sin m\varphi).$$

We note that the Fourier coefficients  $\beta_m$  and  $\gamma_m$  converge to zero when  $m$  tends to infinity. In solving the inverse problem (3.1), we replace  $r(\varphi)$  by the cut-off approximation  $r^M(\varphi)$  for some  $M \in \mathbb{N}$

$$(3.20) \quad r^M(\varphi) := \beta_0 + \sum_{m=1}^M (\beta_m \cos m\varphi + \gamma_m \sin m\varphi).$$

Using this parametrization, the inverse problem is to reconstruct the parameters  $\alpha_o, \varrho_1, \varrho_2, \beta_m, m = 0, \dots, M$  and  $\gamma_m, m = 1, \dots, M$ .

The main advantage using this parametrization of the cross-section is that, for regular shapes (e.g. circles, ellipses) the Fourier coefficients decay to zero very quickly. Therefore, only a few number of Fourier coefficients need to be reconstructed which helps improve the stability of the inverse problem.

In solving the minimization problem, some constraints of the unknown parameters must be taken into account. Firstly, it is obvious that the thermal diffusivity  $\alpha_o$  is bounded by  $\alpha^l$  and  $\alpha^u$  as in (3.2), i.e.

$$(3.21) \quad 0 < \alpha^l \leq \alpha_o \leq \alpha^u.$$

Secondly, we can assume that the object's cross section is not too small or too large. Under this assumption, the radial function should be bounded

$$(3.22) \quad 0 < r^l \leq r(\varphi) \leq r^u, \forall \varphi \in [0, 2\pi].$$

Thirdly, we remark that, as analyzed in [31], the detection can only be possible for shallowly buried objects, say, at most 10 cm deep for common anti-personnel (AP) mines. Hence, the depth of burial  $\varrho_1$  should not be too large. Moreover, since we assume that the soil-surface contains only homogeneous soil, the depth of burial must be positive. More precisely, we have

$$(3.23) \quad 0 < \varrho_1^l \leq \varrho_1 \leq \varrho_1^u < l_3,$$

where  $\varrho_1^l$  is a small positive value which prevents the depth of burial from converging to zero and  $\varrho_1^u$  is the maximum depth of burial at which the object is still detectable.

Finally, concerning the height of the object, we showed in [31] that the effect of the object's height on the soil-surface temperature contrast is very small. The contrasts associated with two values of the height are still distinguishable only if these values do not greater than a certain threshold (e.g. approximately 5 cm for common AP mines). Hence, an estimated value of the height is reliable only in this range, i.e. the following constraints should be added to the estimation problem

$$(3.24) \quad h_3 \leq \varsigma \leq \varsigma^u,$$

where  $\varsigma^u$  is the maximum height of the object at which the estimation is still reliable. Note that this parameter must be chosen so that  $\varrho_1^u + \varsigma^u < l_3$ .

To finish this section, let us calculate the derivatives of  $\mathcal{F}_h$  with respect to the new variables. Using the results of the previous section, it is sufficient to calculate the derivatives of  $\alpha_i(k)$  with respect to them. Denote by  $\alpha_{12}(x_1, x_2)$  the coefficient on a horizontal surface of the soil domain across the object. For simplicity, we assume that the height of the object is not less than the corresponding grid size, that is,  $\varrho_2 - \varrho_1 \geq h_3$ . Furthermore, if we denote by  $\gamma_i^1(k_1, k_2)$  the projection of  $\omega_i(k)$  on the surface  $\Gamma^1$ , and  $\alpha_{12}^i(k_1, k_2), 1 \leq k_i \leq N_i - 1, i = 1, 2, 3$ , specified by

$$\alpha_{12}^i(k_1, k_2) = \frac{1}{h_1 h_2} \int_{\gamma_i^1(k_1, k_2)} \alpha_{12}(x_1, x_2) dx_1 dx_2$$

and suppose that the location of the top surface of the object falls into the grid intervals  $[(k'_3 - 0.5)h_3, (k'_3 + 0.5)h_3)$  and  $[k^*_3h_3, (k^*_3 + 1)h_3)$ , while the bottom surface falls into the intervals  $[(k''_3 - 0.5)h_3, (k''_3 + 0.5)h_3)$  and  $[k^{**}_3h_3, (k^{**}_3 + 1)h_3)$ . That is,

$$(k'_3 - 0.5)h_3 \leq \varrho_1 < (k'_3 + 0.5)h_3, \quad (k''_3 - 0.5)h_3 \leq \varrho_2 < (k''_3 + 0.5)h_3, \\ k^*_3h_3 \leq \varrho_1 < (k^*_3 + 1)h_3, \quad k^{**}_3h_3 \leq \varrho_2 < (k^{**}_3 + 1)h_3,$$

then the average values  $\alpha_i(k)$ ,  $1 \leq k_1 \leq N_1 - 1$ ,  $1 \leq k_2 \leq N_2 - 1$ ,  $0 \leq k_3 \leq N_3 - 2$ , can be represented as

$$\alpha_i(k) = \begin{cases} \alpha_s, & \text{if } k_3 < k'_3, \\ \frac{1}{h_3} \{ \alpha_s[\varrho_1 - (k'_3 - 0.5)h_3] + \alpha^i_{12}(k_1, k_2)[(k'_3 + 0.5)h_3 - \varrho_1] \}, & \text{if } k_3 = k'_3, \\ \alpha^i_{12}(k_1, k_2), & \text{if } k'_3 + 1 \leq k_3 \leq k''_3 - 1, \\ \frac{1}{h_3} \{ \alpha^i_{12}(k_1, k_2)[\varrho_2 - (k''_3 - 0.5)h_3] + \alpha_s[(k''_3 + 0.5)h_3 - \varrho_2] \}, & \text{if } k_3 = k''_3, \\ \alpha_s, & \text{if } k_3 > k''_3, \end{cases}$$

for  $i = 1, 2$  and

$$\alpha_3(k) = \begin{cases} \alpha_s, & \text{if } k_3 < k^*_3, \\ \frac{1}{h_3} \{ \alpha_s[\varrho_1 - k^*_3h_3] + \alpha^3_{12}(k_1, k_2)[(k^*_3 + 1)h_3 - \varrho_1] \}, & \text{if } k_3 = k^*_3, \\ \alpha^3_{12}(k_1, k_2), & \text{if } k^*_3 + 1 \leq k_3 \leq k^{**}_3 - 1, \\ \frac{1}{h_3} \{ \alpha^3_{12}(k_1, k_2)[\varrho_2 - k^{**}_3h_3] + \alpha_s[(k^{**}_3 + 1)h_3 - \varrho_2] \}, & \text{if } k_3 = k^{**}_3, \\ \alpha_s, & \text{if } k_3 > k^{**}_3. \end{cases}$$

The derivatives of  $\alpha_i$ ,  $i = 1, 2$ , with respect to  $\varrho_1$  and  $\varrho_2$  are given by

$$\frac{\partial \alpha_i(k)}{\partial \varrho_1} = \begin{cases} \frac{1}{h_3} [\alpha_s - \alpha^i_{12}(k_1, k_2)], & \text{if } k_3 = k'_3, \\ 0, & \text{otherwise,} \end{cases} \\ \frac{\partial \alpha_i(k)}{\partial \varrho_2} = \begin{cases} \frac{1}{h_3} [\alpha^i_{12}(k_1, k_2) - \alpha_s], & \text{if } k_3 = k''_3, \\ 0, & \text{otherwise.} \end{cases}$$

Similar formulas are obtained for  $\alpha_3$ . On the other hand, assuming that  $\alpha_o \neq \alpha_s$ , we obtain the derivative with respect to  $\alpha_o$ :

$$\frac{\partial \alpha_i(k)}{\partial \alpha_o} = \Delta h \frac{\alpha_s - \alpha_i(k)}{\alpha_s - \alpha_o}.$$

For the geometric parameters  $\beta_m$  and  $\gamma_m$ , it is difficult to obtain analytic formulas for the derivatives of  $\alpha_i(k)$  with respect to these parameters. Therefore, we approximate them by finite difference quotients. Since the coefficient does not depend on time, this approximation method is much faster than using finite difference approximations directly for the objective functional. Then using the chain rule, we obtain the derivatives of the objective functional  $\mathcal{F}_h$  with respect to the new variables. Note that, the height of the object is given by  $\varsigma = \varrho_2 - \varrho_1$ .

## 4. NUMERICAL RESULTS

This section consists of two parts. In the first part, we validate the proposed thermal model (2.12) using experimental data measured in a dummy minefield. In the second part, we illustrate the performance of the inverse problem with reconstruction results for both simulated and experimental data.

**4.1. Validation of the forward thermal model.** In this section, we show that the proposed thermal model (2.12) can be used in practice to approximate the evolution of the ground thermal signature with the presence of buried landmines. For this purpose, we compare numerical simulations to experimental data. The experimental data used in this paper was acquired in a test minefield in the Netherlands in 2001. The minefield was a box of sandy soil with several buried landmines and other test objects. The mines were filled with a material having the same properties as TNT, see Table 1. For a detailed description of the experiment setup and the minefield we refer the reader to [9].

IR images were acquired by a Quantum Well Infrared Photo detector (QWIP). The temperature resolution of the IR sensor is 0.03 K. Moreover, a weather station was used to measure meteorological data such as solar irradiance, sky irradiance, air temperature and wind speed. Before applying the algorithms to the

Material	Conductivity W/(m K)	Density kg/m <sup>3</sup>	Heat capacity J/(kg K)	Diffusivity m <sup>2</sup> /s
Sandy soil	0.75	1650	710	$6.402 \times 10^{-7}$
TNT	0.2	1170	1500	$1.1396 \times 10^{-7}$

TABLE 1. Thermal characteristics of sandy soil and TNT.

IR data set, a pre-processing chain, consisting of (i) radiometric calibration, (ii) temporal co-registration, (iii) atmospheric correction, (iv) apparent temperature conversion, and (v) inverse perspective (ground) projection, was applied to the acquired IR images. For these steps, we refer to [31]. In this work, we assume that the measured IR images represent the ground-surface temperature. For the simplicity of analysis, the IR images were spatially interpolated with the resolution of  $0.01 \times 0.01$  (m<sup>2</sup>).

As mentioned in Section 2, the input parameters (the soil thermal diffusivity, the soil-surface boundary condition) of the thermal model (2.12) should be estimated using *in situ* soil-temperature measurements. For this data set, the estimated soil thermal diffusivity ( $6.420 \times 10^{-7}$  m<sup>2</sup>/s) is very close to the reference value ( $6.402 \times 10^{-7}$  m<sup>2</sup>/s), see [31]. Hence, the latter is used in the following validation. The estimated value of the parameter  $p$  in the air-soil interface boundary condition is  $p = 7.01 \times 10^{-6}$  and the function  $q(t)$  is depicted in Figure 3(a).

In the following, we compare simulations using the thermal model (2.12) with measured data for two different AP mines of different sizes. Their codes in the

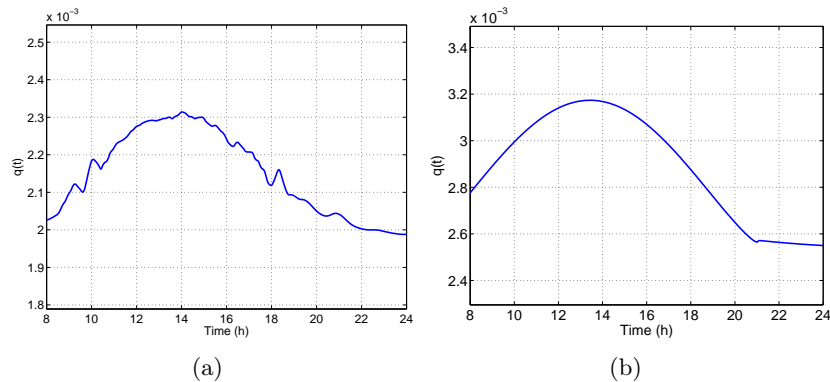


FIGURE 3. The function  $q(t)$ : (a) Experimental data; (b) Simulated data.

experiment were B82 and C49, respectively. Their characteristics are given in Table 2. More validation results were given in [34, 31].

Code	Type	Shape	Height	Diameter	Depth of burial
B82	AP (NR22C1)	cylindrical	0.053 m	0.062 m	0.01 m
C49	AP (PMN)	cylindrical	0.048 m	0.117 m	0.01 m

TABLE 2. Properties of the test mines.

To simulate the soil temperature, a volume of 40 cm by 40 cm by 50 cm around each mine was considered. The locations of the mines were provided by the ground truth. The discretization step was set to be 0.01 m in each direction for the compatibility with the resolution of the measured IR images and the time step was chosen to be 60 seconds.

As analyzed in Section 2, we should start the simulations around sunrise or sunset in order to have a good approximation of the initial condition. The IR images show that the heat equilibrium happened around 8:00 for this experiment. The soil temperature at this time instant was approximated by interpolating the soil temperature at different depths measured by thermocouples.

Figures 4 and 5 depict the simulated and measured soil-surface temperature above the mines (the left figures), in the homogeneous soil areas (the middle figures) and the temperature contrasts of the mines (the right figures) which are calculated as the difference between the soil-surface temperature above the mines and that of the background.

The figures show that the simulated soil-surface temperature and contrast between the mines and the soil approximate well the measured data. This confirms the validity of the thermal model (2.12) in practical situations.

From the figures we can also see that the temperature contrast depends on the size of the buried mines. Moreover, in [31], we also showed that several factors

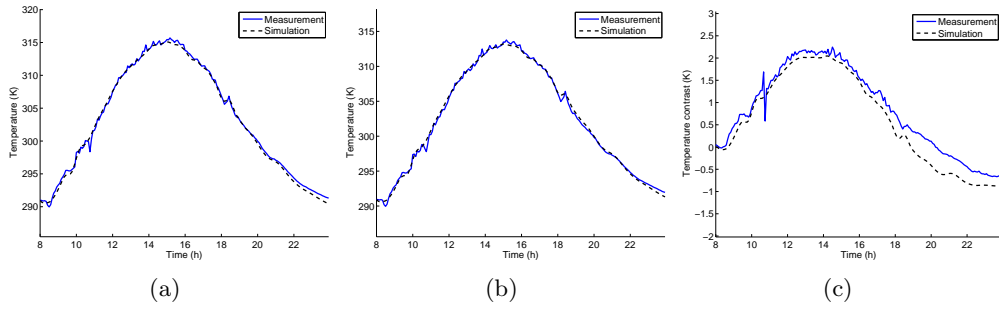


FIGURE 4. Comparison of the simulated and measured background temperature for mine B82: (a) Temperature above the mine; (b) Temperature in a homogeneous soil area; (c) Temperature contrast.

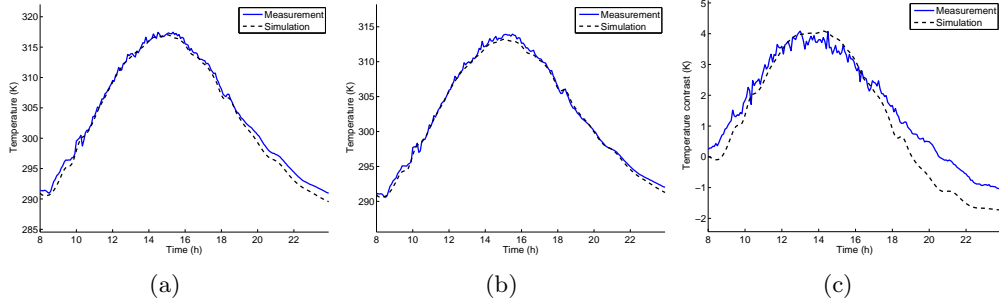


FIGURE 5. Comparison of the simulated and measured background temperature for mine C49: (a) Temperature above the mine; (b) Temperature in a homogeneous soil area; (c) Temperature contrast.

have effect on the soil-surface temperature contrast such as the soil type, the depth at which the mines are buried and the weather conditions.

**4.2. Results of the inverse problem.** Having the validated forward model (2.12), the next step is to test the performance of the proposed algorithm for the inverse problem. In the following, we show for some numerical examples using both simulated and real data.

*Simulated data.* We first test the proposed algorithm for simulated data. Keeping in mind the application in real situations, we choose similar parameters as in the aforementioned experiment. A cylindrical mine of radius 0.04 m and height 0.05 m was buried in the middle of a sandy soil volume at 0.015 m deep. The size of the soil domain was set to be  $0.34 \times 0.34 \times 0.4$  ( $\text{m}^3$ ) and the time interval of analysis was chosen to be  $t_e = 16$  (h) (from 8:00 till 24:00). The discretization grid sizes were chosen as  $h = (0.01, 0.01, 0.01)$  (m) and  $\Delta t = 300$  (s) resulting in

$35 \times 35 \times 41$  space grid points and 193 time steps. We note that due to the small sizes of landmines, the spatial grid sizes should not be chosen too large while, due to the stability of the splitting scheme (2.35), the time step can be more freely chosen.

The initial condition was set to be  $g(x) = 293$  (K). The parameters  $p$  and  $q(t)$  were calculated through weather conditions, see [34]. In this example, we have  $p = 9.2265 \times 10^{-6}$  and  $q(t)$  is depicted in Figure 3(b).

In order to avoid the so-called *inverse crime*, we used an explicit finite difference method to simulate the measured data. Then a random noise of magnitude of 0.1 K was added to the simulated data. We remark that the soil-surface temperature contrast is generally small, say, less than a few degrees Kelvin, see [33]. Therefore, the noise level of 0.1 K is large in this situation, especially when the mine is deeply buried.

For the star-shaped representation (3.19), we need to know the point  $x^0$  which must be inside the cross-section of the object. To estimate this point, we make use of the anomaly detection technique proposed in [35]. This technique not only helps detect the location of an anomaly but also provides a rough estimate of the cross-section, see Figures 6(a) and 7(a). Therefore, the detected mask can be used as an initial guess of the cross-section. In this test, we obtained  $x^0 = (0.17, 0.17)'$ .

The first test of the algorithm was done with only four unknowns representing the depth of burial, height, radius and thermal diffusivity. In this case, we assumed that the cross-section of the mine was circular with the center at  $x^0$ . The reconstruction result is depicted in Figure 6. In the figure we also plot the initial guess.

From the figure we can say firstly that the algorithm converges very quickly. This is the benefit of using a small number of unknowns. The use of a small number of unknowns also plays the role of regularization which makes the algorithm stable although we do not use any other regularization techniques. Secondly, the depth, the shape and the thermal diffusivity of the mine are accurately reconstructed. However, the estimation of the height is not really good. This is due to the fact that the height does not affect so much the soil-surface temperature as mentioned before, see also [34].

To analyze the effect of the initial guess given by the anomaly detection technique, in Figure 7 we plot the reconstruction result using another estimated mask. We can see that after a few iterations, the algorithm also converges to a very good result.

To finish the analysis of the simulated data, let us analyze the effect of the point  $x^0$  to the accuracy of the reconstruction. To do so, we set  $x^0 = (0.18, 0.15)'$ . In this case, since this point is not at the center of the true object, we use three parameters  $\beta_0, \beta_1, \gamma_1$  to represent the cross-section which results six unknowns to be estimated. Note that the anomaly detection technique was not used for this test. Figure 8 shows that the algorithm again provided a very good result. We emphasize that if only one parameter is used for the cross-section, there must be a shift between the exact and the estimated cross-sections. If more number of

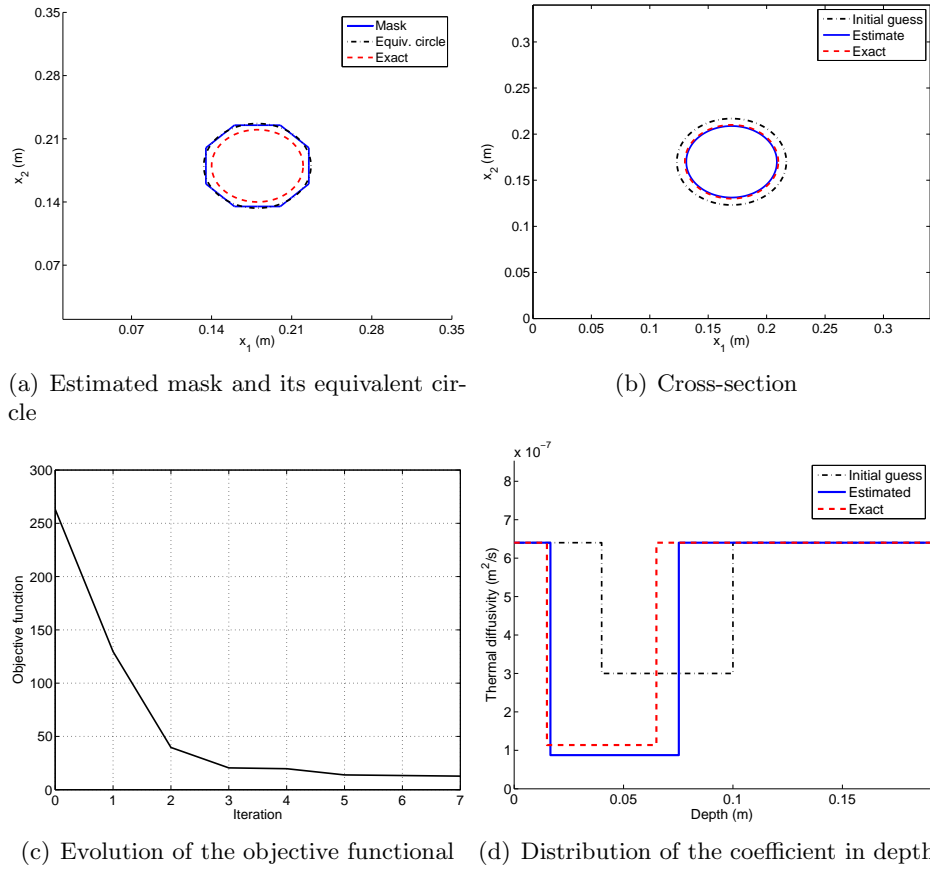
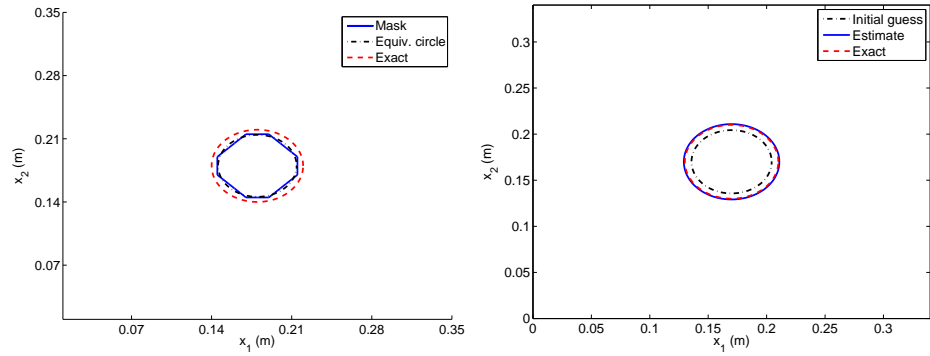


FIGURE 6. Reconstruction result for the simulated mine.

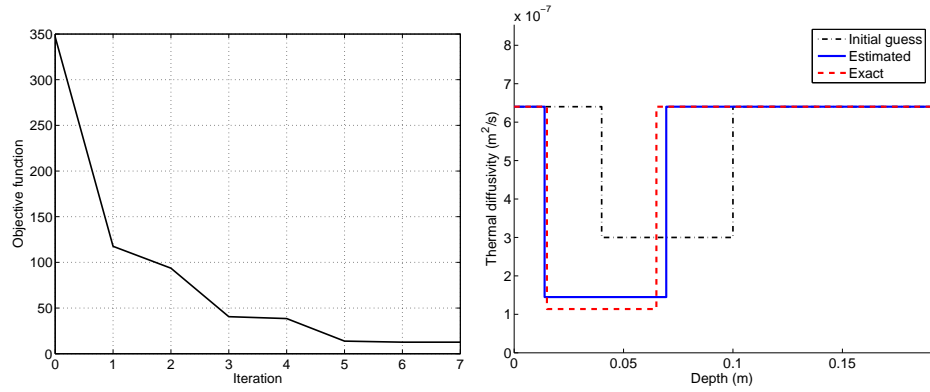
Fourier coefficients are used, it is possible to represent more complicated shapes, but the algorithm becomes less stable. Therefore, if we know *a priori* that the shape is regular, we should use just a few Fourier coefficients.

*Real experimental data.* Using the same algorithm, we obtained the reconstruction results for the experimental mines B82 and C49. The results are depicted in Figure 9 and Figure 10, respectively. It is clear that, due to several types of noise, the results of the experimental data are not as good as those of the simulated data. The estimated cross-sections are larger than the ground truth. However, the depth and the thermal diffusivity are reasonably well reconstructed. These results are comparable to the results of the two-step method given in [31, 35] but the computational cost of this algorithm is only of the same order as the first step of the two-step method.



(a) Estimated mask and its equivalent circle

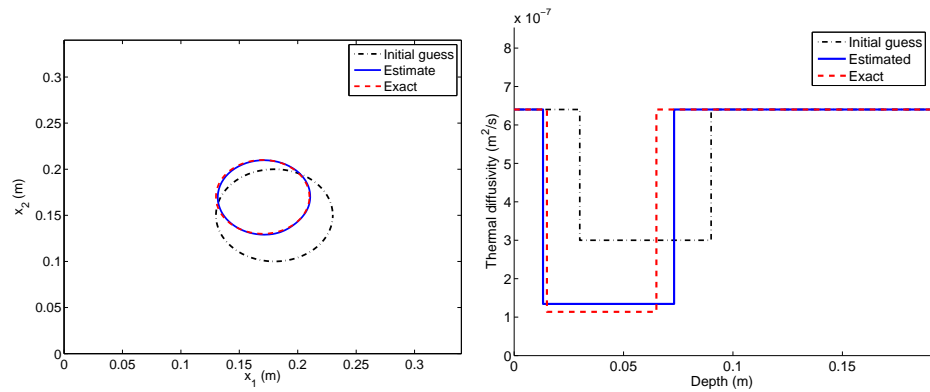
(b) Cross-section



(c) Evolution of the objective functional

(d) Distribution of the coefficient in depth

FIGURE 7. Reconstruction result for the simulated mine with another estimated mask.



(a) Cross-section

(b) Distribution of the coefficient in depth

FIGURE 8. Reconstruction of the simulated mine with  $x^0 = (0.18, 0.15)'$ .

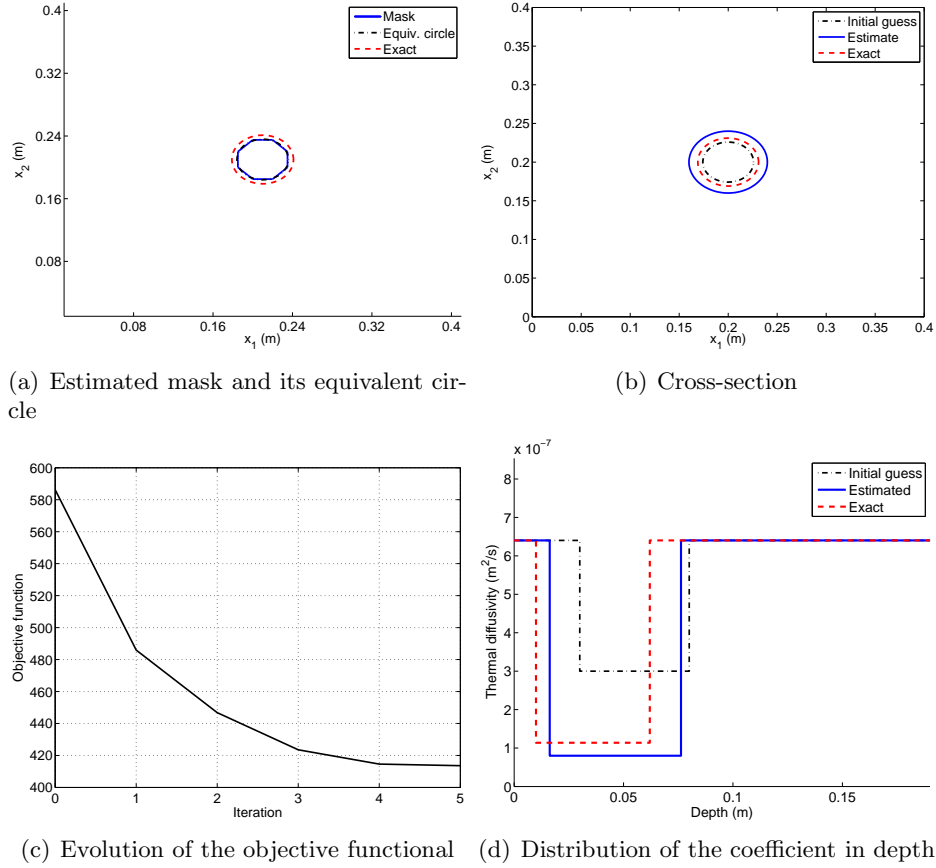


FIGURE 9. Reconstruction result for the mine B82.

### 5. CONCLUSIONS

We have described the mathematical formulation of a thermal model for landmine detection using IR technique and formed an inverse problem for characterizing a buried object by estimating its depth of burial, shape and thermal diffusivity. We have also proposed a new algorithm for the inverse problem by using the star-shaped representation of the object cross-section. Numerical results have shown the good performance of the proposed algorithm.

For further investigations of this problem, other parametrization methods should be used for representing the whole object's shape in order to deal with other types of shape rather than upright cylinders. The finite element method can also be used to solve the forward problem which can allow us to calculate the gradient of the objective functional with respect to geometrical parameters by a more explicit way.

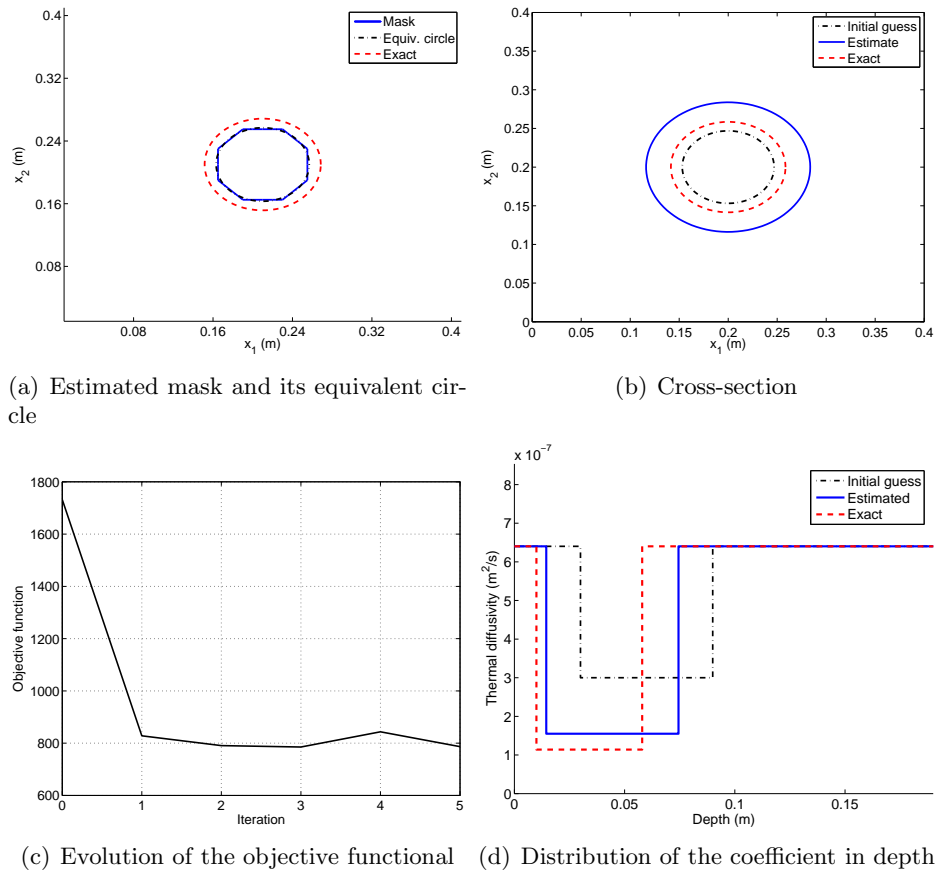


FIGURE 10. Reconstruction result for the mine C49.

## REFERENCES

- [1] R. A. Adams, *Sobolev Spaces*, Academic Press, New York, 1975.
- [2] O. M. Alifanov, *Inverse Heat Transfer Problems*, Springer Verlag, 1995.
- [3] O. M. Alifanov, E. A. Artiukhin and S. V. Rumiantsev, *Extreme Methods for Solving Ill-Posed Problems With Applications to Inverse Heat Transfer Problems*. Begell House Publishers, 1995.
- [4] J. V. Beck, B. Blackwell, C. R. St. Clair Jr., *Inverse Heat Conduction: Ill-Posed Problems*, Wiley-Interscience, 1985.
- [5] H. S. Carslaw and J. C. Jaeger, *Conduction of Heat in Solids*, Oxford University Press, Oxford, second edition, 1959.
- [6] F. Cremer, N. T. Thành, L. Yang, and H. Sahli, Stand-off thermal IR minefield survey, system concept and experimental results, In R. S. Harmon, J. T. Broach, and J. H. Holloway, Jr., editors, *Proceedings of SPIE 5794, Detection and Remediation Technologies for Mine and Minelike Targets X*, pages 209–220, 2005.
- [7] Dinh Nho Hào, A Noncharacteristic Cauchy Problem for Linear Parabolic Equations and Related Inverse Problems I: Solvability, *Inverse Problems* **10** (1994), 295–315.
- [8] Dinh Nho Hào, *Methods for Inverse Heat Conduction Problems*. Peter Lang Verlag, Frankfurt/Main, Bern, New York, Paris, 1998.

- [9] W. de Jong, H. A. Lensen, and Y. H. Janssen, Sophisticated test facility to detect land mines, In A. C. Dubey, J. F. Harvey, J. T. Broach, and R. E. Dugan, editors, *Proceedings of SPIE 3710, Detection and Remediation Technologies for Mine and Minelike Targets IV*, pages 1409–1418, Orlando, FL, Apr 1999.
- [10] J. Douglas and H. Rachford, On the numerical solution of the heat conduction problems in two and three space variables, *Trans. Amer. Math. Soc.* **82** (1956), 421–439.
- [11] A. Elayyan and V. Isakov, On uniqueness of recovery of the discontinuous conductivity coefficient of a parabolic equation, *SIAM J. Appl. Math.* **28**(1) (1997), 49–59.
- [12] S. Gutman, Identification of discontinuous parameters in flow equations, *SIAM J. Control Optim.* **28** (5) (1990), 1049–1060.
- [13] S. Gutman and J. Ha, Identifiability of piecewise constant conductivity in a heat conduction process, *SIAM J. Control Optim.* **46** (2) (2007), 694–713 (electronic).
- [14] S. Gutman and J. Ha, Parameter identifiability for heat conduction with a boundary input, *Math. Comput. Simulation* **79**(7) (2009), 2192–2210.
- [15] N. S. Hoang and A. G. Ramm, An inverse problem for a heat equation with piecewise-constant thermal conductivity, *J. Math. Phys.* **50**(6) (2009), 063512, 5pp.
- [16] P. A. M. Jacobs, *Thermal Infrared Characterization of Ground Targets and Backgrounds*, SPIE Optical Engineering Press, Bellingham (WA), USA, 1996.
- [17] K. Khanafer, K. Vafai, and B. A. Baertlein, Effects of thin metal outer case and top air gap on thermal IR images of buried antitank and antipersonnel land mines, *IEEE Transactions on Geoscience and Remote Sensing* **41**(1) (2003), 123–135.
- [18] O. A. Ladyzhenskaya, *The Boundary Value Problems of Mathematical Physics*, Springer-Verlag, New York, 1985.
- [19] P. López, *Detection of Landmines from Measured Infrared Images using Thermal Modelling of the Soil*, PhD thesis, University of Santiago de Compostela, Spain, 2003.
- [20] P. López, L. Van Kempen, H. Sahli, and D. C. Ferrer, Improved thermal analysis of buried landmines, *IEEE Transactions on Geoscience and Remote Sensing* **4** (9) (2004), 1965–1975.
- [21] G. I. Marchuk, *Methods of Numerical Mathematics*, Springer-Verlag, New York, 1975.
- [22] G. I. Marchuk, Splitting and alternating direction methods, In *Handbook of numerical analysis, Vol. I*, Handb. Numer. Anal., I, pages 197–462. North-Holland, Amsterdam, 1990.
- [23] The Math Works Inc, *Optimization Toolbox for Use with Matlab: User's Guide*, 3 edition, 1990–2004.
- [24] A. Muscio and M. A. Corticelli, Land mine detection by infrared thermography: reduction of size and duration of the experiments, *IEEE Transactions on Geoscience and Remote Sensing* **42**(9) (2004), 1955–1964.
- [25] D. W. Peaceman and H. H. Rachford Jr., The numerical solution of parabolic and elliptic differential equations, *J. Soc. Indust. Appl. Math.* **3** (1955), 28–41.
- [26] A. A. Samarskii, *Theory of the Difference Schemes*, Nauka, Moscow, 1983.
- [27] A. A. Samarskii, *The Theory of Difference Schemes*, Pure and Applied Mathematics. Marcel Dekker, New York, 2001.
- [28] A. A. Samarskii, P. P. Matus, and P. N. Vabishchevich, *Difference Schemes with Operator Factors*, Mathematics and its Applications. Kluwer Academic Publishers, Boston–Dordrecht–London, 2002.
- [29] A. A. Samarskii and P. N. Vabishchevich, *Computational Heat Transfer. Volume 1: Mathematical Modelling*, John Wiley & Sons, Chichester, 1995.
- [30] A. A. Samarskii and P. N. Vabishchevich, *Computational Heat Transfer. Volume 2: The Finite Difference Methodology*, John Wiley & Sons, Chichester, 1995.
- [31] N. T. Thành, *Infrared Thermography for the Detection and Characterization of Buried Objects*, PhD thesis, Vrije Universiteit Brussel, Brussels, Belgium, 2007.
- [32] N. T. Thành, D. N. Hào, and H. Sahli, Infrared thermography for landmine detection. In R. I. Hammoud, editor, *Augmented Vision Perception in Infrared. Algorithms and Applied Systems*, pages 3–36. Springer, 2009.

- [33] N. T. Thành, H. Sahli, and D. N. Hào, Detection and characterization of buried landmines using infrared thermography, *Inverse Probl. Sci. Eng.* **19** (2011), 281–307.
- [34] N. T. Thành, H. Sahli, and D. N. Hào, Finite difference methods and validity of a thermal model for landmine detection with soil property estimation. *The IEEE Transactions on Geoscience and Remote Sensing* **45**(3) (2007), 656–674.
- [35] N. T. Thành, H. Sahli, and D. N. Hào, Infrared thermography for buried landmine detection: inverse problem setting, *The IEEE Transactions on Geoscience and Remote Sensing* **46**(12) (2008), 3987–4004.
- [36] K. Watson, Geologic applications of thermal infrared images, *Proceedings of the IEEE* **63**(1) (1975), 128–137.

JOHANN RADON INSTITUTE FOR COMPUTATIONAL AND APPLIED MATHEMATICS (RICAM)  
AUSTRIAN ACADEMY OF SCIENCES, ALTENBERGERSTRASSE 69, A-4040 LINZ, AUSTRIA  
*E-mail address:* `trung-thanh.nguyen@ricam.oeaw.ac.at`

HANOI INSTITUTE OF MATHEMATICS  
18 HOANG QUOC VIET ROAD, 10307 HANOI, VIETNAM  
*E-mail address:* `hao@math.ac.vn`

VRIJE UNIVERSITEIT BRUSSEL, DEPARTMENT OF ELECTRONICS AND INFORMATICS  
PLEINLAAN 2, 1050 BRUSSELS, BELGIUM  
*E-mail address:* `hichem.sahli@etro.vub.ac.be`